Geochemistry, Geophysics, Geosystems®

AGU ADVANCING EARTH AND SPACE SCIENCE

RESEARCH ARTICLE
10.1029/2021GC010324

Geodynamic and Isotopic Constraints on the Genesis of Kimberlites, Lamproites and Related Magmas From the Finnish Segment of the Karelian Craton

Hayden Dalton[1], Andrea Giuliani[1,2], Janet Hergt[1], David Phillips[1], Hugh O'Brien[3], Maxim D. Ballmer[4], Roland Maas[1], and Jon Woodhead[1]

[1]KiDs (Kimberlites and Diamonds) Research Group, School of Geography, Earth and Atmospheric Sciences, The University of Melbourne, Parkville, VIC, Australia, [2]Department of Earth Sciences, Institute of Geochemistry and Petrology, ETH Zurich, Zurich, Switzerland, [3]Geological Survey of Finland, Espoo, Finland, [4]Department of Earth Sciences, University College London, London, UK

Key Points:

- New radiogenic isotope data reveals distinct sources and petrogenesis for three occurrences of kimberlite and related magmatism in Finland
- Kimberlite magmatism in Finland is synchronous with initiation and completion of Rodinia's break-up with potential links to mantle plumes
- The primitive source region of the Kaavi-Kuopio kimberlites was significantly modified by increasing incorporation of recycled material

Supporting Information:

Supporting Information may be found in the online version of this article.

Correspondence to:

H. Dalton and A. Giuliani,
hayden.dalton@unimelb.edu.au;
andrea.giuliani@erdw.ethz.ch

Citation:

Dalton, H., Giuliani, A., Hergt, J., Phillips, D., O'Brien, H., Ballmer, M. D., et al. (2022). Geodynamic and isotopic constraints on the genesis of kimberlites, lamproites and related magmas from the Finnish segment of the Karelian craton. *Geochemistry, Geophysics, Geosystems*, *23*, e2021GC010324. https://doi.org/10.1029/2021GC010324

Received 4 JAN 2022
Accepted 16 JUN 2022

Author Contributions:

Conceptualization: Hayden Dalton
Data curation: Hayden Dalton, Roland Maas, Jon Woodhead
Formal analysis: Hayden Dalton, Roland Maas, Jon Woodhead
Funding acquisition: David Phillips
Investigation: Hayden Dalton, Andrea Giuliani, Maxim D. Ballmer
Methodology: Hayden Dalton, Roland Maas, Jon Woodhead
Project Administration: Hayden Dalton, Andrea Giuliani, David Phillips

Abstract Despite the scientific and economic significance of kimberlites and related magmas, their origin is unclear. Here, we address this issue using whole-rock and perovskite-derived Sr-Nd-Hf isotopes for the three occurrences of kimberlite, lamproites and ultramafic lamprophyres (UMLs) in Finland. Mesoproterozoic olivine lamproites at Lentiira-Kuhmo and UMLs at Kuusamo have different isotopic signatures yet were emplaced contemporaneously at 1,200 Ma in response to an extensional regime linked to the Baltica-Laurentia breakup. The low $\varepsilon Nd_{(i)}$ and $\varepsilon Hf_{(i)}$ values of the olivine lamproites are consistent with an enriched subcontinental lithospheric mantle (SCLM) source while UML compositions are intermediate between those of typical kimberlites and lamproites and are interpreted to reflect mixing of asthenospheric melts and ~10%–15% of melts sourced from metasomatized SCLM. The ~750 Ma Kuusamo kimberlites, are probably linked to the mantle plume activity that initiated Rodinia's break-up, exhibiting homogenous isotopic compositions which mirror the prominent Geodynamic and Source Constraints for ~1,200 Ma Olivine Lamproite and Ultramafic Lamprophyre Magmatism in Eastern Finland (PREMA)-like signature of kimberlites globally. By contrast, ~620–585 Ma Kaavi-Kuopio kimberlites show limited range in $\varepsilon Nd_{(i)}$ and $^{87}Sr/^{86}Sr_{(i)}$ but have remarkably heterogeneous $\varepsilon Hf_{(i)}$ (+6.5 to −6.3) with a temporal trend toward lower $\varepsilon Hf_{(i)}$ values. While the Kuusamo kimberlites erupted during the early stage of continental break-up, the Kaavi-Kuopio kimberlites were emplaced when Rodinia break-up was completed, coeval with formation of the Central Iapetus large igneous province. Magmas forming the Kaavi-Kupio kimberlites may have formed from an upwelling mantle source similar to PREMA modified by increasing incorporation (up to 10%) of recycled crustal material through time accounting for the trend toward lower $\varepsilon Hf_{(i)}$ in these kimberlites.

Plain Language Summary Kimberlites and related rocks are of great economic and scientific importance as they are some of the deepest derived mantle melts (> 150–200 km) and carry a diverse cargo of mantle material, including diamonds. In this study, we utilize new radiogenic isotope data combined with geochemical modeling and existing geodynamic reconstructions to propose genetic models for the emplacement of kimberlites, ultramafic lamprophyres (UMLs) and olivine lamproites in Finland. The UMLs and olivine lamproites may be genetically related given their close temporal overlap and their compositions testify to progressively increasing contributions by geochemically enriched lithospheric mantle sources. We propose that kimberlite activity in Finland is fueled by melting of deep mantle sources that bookends both the onset and completion the break-up of an ancient supercontinent, Rodinia. This supercontinent disintegration and, potentially, kimberlite activity, was likely driven by the deep mantle upwellings, or plumes, beneath the region. In addition, our modeling suggests the unique, isotopic evolution of the mantle source for the youngest Finnish kimberlites occurrence reflects progressive incorporation of ancient, recycled material into their mantle plume source.

1. Introduction

Kimberlites are rare, small-volume igneous rocks emplaced within ancient continental blocks from at least 2.8 Ga to the earliest Holocene (Giuliani & Pearson, 2019; Heaman et al., 2019; Mitchell, 1986; Tappe et al., 2018). Kimberlites have attracted significant interest because their rich cargo of xenolithic material (including diamonds)

Resources: Andrea Giuliani, Janet Hergt, David Phillips, Hugh O'Brien
Software: Hayden Dalton
Supervision: Andrea Giuliani, Janet Hergt, David Phillips, Hugh O'Brien
Visualization: Hayden Dalton
Writing – original draft: Hayden Dalton
Writing – review & editing: Hayden Dalton, Andrea Giuliani, Janet Hergt, David Phillips, Hugh O'Brien, Maxim D. Ballmer, Roland Maas

suggests they are derived from deep mantle magma sources not tapped by any other type of terrestrial magmatic rocks. Our understanding of kimberlite petrogenesis, from their mantle source to eruption through Earth's crust, has improved over the last few decades, yet much is still unknown.

The debate around the ultimate source region of kimberlites incorporates a spectrum of hypotheses. For example, some workers have proposed kimberlite derivation from domains in the subcontinental lithospheric mantle (SCLM) which were metasomatized by asthenosphere-derived melts with ocean island basalt (OIB)-like characteristics (e.g., Becker and le Roex, 2006; Helmstaedt & Gurney, 1997; le Roex et al., 2003; Tainton & McKenzie, 1994). A sub-lithosphere origin for kimberlites has become the more prevalent hypothesis in recent years, supported by an extensive body of evidence, including radiogenic isotope signatures (e.g., Giuliani et al., 2021; Smith, 1983; Tappe, Romer, et al., 2017; Woodhead et al., 2009; Woodhead et al., 2019), entrainment of super-deep diamonds hosting mineral inclusions from the mantle transition zone or lower mantle (Harte & Harris, 1994; Kaminsky, 2012; Pearson et al., 2014; Stachel, 2001), and a geographic association of kimberlite provinces with large low shear wave velocity provinces (LLSVPs), which represent seismically anomalous thermochemical structures at the base of the mantle from which mantle plumes stem (e.g., Burke, 2011; Torsvik et al., 2010). The occurrence of kimberlites along age-progressive hot-spot tracks which continue as OIB in oceanic basins (Heaman & Kjarsgaard, 2000) supports a deep plume-related genesis for at least some kimberlites. Regardless of the exact depth of kimberlite genesis below the lithosphere-asthenosphere boundary (LAB), the source region(s) is likely to represent a mix of multiple components. For example, some studies have indicated the presence of "ancient", "refractory" or "primordial" components in the source of these rocks (e.g., Giuliani et al., 2021; Nakanishi et al., 2021; Tappe, Budde, et al., 2020; Woodhead et al., 2019), as well as the incorporation of "subducted/recycled" and "enriched" material into the kimberlite source region (e.g., Giuliani et al., 2022; Nowell et al., 2004; Tappe et al., 2013; Tovey et al., 2021; Woodhead et al., 2019).

In addition to the ongoing discussion pertaining to the source of kimberlites, the causes of melt generation and eruption remain contentious. Spatiotemporal relationships with diverse geodynamic events have been used to suggest kimberlitic magmatism may have been caused by deep mantle plumes (perhaps emanating from the core-mantle boundary), by distal subduction, by rifting and/or continental migration and by collision (e.g., Heaman & Kjarsgaard, 2000; Jelsma et al., 2009; McCandless, 1999; Stern et al., 2016; Tappe, Brand, et al., 2017; Tappe et al., 2018; Torsvik et al., 2010). It is unclear whether these hypotheses are all valid and can be applied to different kimberlite provinces, or if all kimberlite occurrences can be explained by one unifying model.

Southern Africa, Siberia and Canada host the largest number of economic kimberlite bodies and efforts to unravel kimberlite petrogenesis have therefore largely focused on these regions. However, much can be learned from examining new regions as the different tectonic settings of such areas can reveal more nuanced information on kimberlite genesis and provide a point of context from which we can make additional comparisons. It also remains unclear, the extent to which kimberlites lie on a genetic continuum between other ultramafic alkaline rock types such as olivine lamproites and ultramafic lamprophyres (UMLs) which may themselves be related to each other (e.g., Sarkar et al., 2021; Shaikh et al., 2017; Tappe et al., 2008). It is therefore important to examine regions in which these lithologies spatially and/or temporally overlap. In this study we contribute to the above petrogenetic discussions and report new whole-rock and perovskite-derived Sr-Nd-Hf radiogenic isotope data for samples ($n = 24$) from the three prominent occurrences of kimberlite, olivine lamproite and ultramafic lamprophyre magmatism in Finland for which the emplacement ages, petrography and geochemistry had been previously characterized (see below). We integrate these new results with previous data and available estimates for the Meso- and Neoproterozoic paleo-positions of Finland and the Baltic Shield to constrain the composition of the source region and deduce the possible triggers of kimberlite and related magmatism in this region.

2. Samples and Geological Setting

The samples ($n = 24$) used in this study were collected from drill-cores stored at the National Drill Core Archive of the Geological Survey of Finland (GTK) and are listed in Table 1. Samples were selected from all available hypabyssal (i.e., subvolcanic magmatic) material from each of the three prominent periods of kimberlite and related activity in Finland to characterize the evolution of magmatism in the region.

The first period of kimberlite and related alkaline ultramafic magmatism in Finland is represented by olivine lamproite pipes and dikes emplaced at Lentiira and Kuhmo in eastern Finland, which are contemporaneous

Geochemistry, Geophysics, Geosystems

10.1029/2021GC010324

Table 1
Summary of Initial Nd, Sr and Hf Isotope Compositions for Kimberlite and Related Rocks in This Study

Field/Cluster	Intrusion name	Sample id	Core depth (m)	Sample type	Age (Ma)[a]	$^{143}Nd/^{144}Nd_{(i)}$	±2se	$\varepsilon Nd_{(i)}$[b]	$^{176}Hf/^{177}Hf_{(i)}$	±2se	$\varepsilon Hf_{(i)}$[b]	$\Delta\varepsilon Hf_{(i)}$[c]	$^{87}Sr/^{86}Sr_{(i)}$	±2se
Kaavi-Kuopio	Pipe 1	1.106	8.15	Whole-Rock	620	0.511898	8	1.2	0.282578	6	6.5	2.5		
	Pipe 1	1.102	16.66	Whole-Rock	620	0.511871	15	0.7	0.282461	7	2.4	−0.8		
	Pipe 2	2.151	13.21	Perovskite	593	0.511912	8	0.8					0.703200	12
	Pipe 3	3.123	24.24	Whole-Rock	584	0.511841	11	−0.8	0.282308	6	−3.9	−5.0		
	Pipe 3	3.96	36.36	Perovskite	584	0.511929	13	0.9					0.703005	14
	Pipe 5	5.7	64.45	Whole-Rock	605	0.511948	9	1.8	0.282416	7	0.5	−4.4		
	Pipe 5	5.7	64.45	Perovskite	605	0.511951	7	1.9					0.703329	13
	Pipe 5	5.8	74.25	Whole-Rock	605	0.511874	9	0.4	0.282322	8	−2.9	−5.7		
	Pipe 9	9.4	40.55	Whole-Rock	591	0.511868	13	−0.1	0.282234	6	−6.3	−8.5		
	Pipe 9	9.2	30.98	Perovskite	591	0.511976	8	2.0					0.703305	12
	Pipe 14	14.07	58.77	Whole-Rock	585	0.511882	7	0.03	0.282267	5	−5.3	−7.6		
Kuusamo	Kalettomanpuro (KP)	KP-01-04	93.5	Perovskite	747	0.511834	13	3.2	0.282487	6	5.2	−1.5	0.702551	19
	Kasma 45	KAS45-07	13.3	Perovskite	734	0.511837	10	2.9	0.282495	7	5.4	−1.5	0.702524	17
	Kasma 45	KAS45-07	13.3	Perovskite	734	0.511826	10	2.7	0.282503	6	4.8	−1.0	0.702660	18
	Kasma 45	KAS45-01	50.4	Perovskite	745	0.511843	12	3.3	0.282488	10	5.4	−1.2	0.702525	14
	Kasma 47	KAS47-02	28.6	Whole-Rock	741	0.511816	14	2.7	0.282469	9	4.5	−1.8		
	Kasma 47	KAS47-02	28.8	Whole-Rock	747	0.511812	8	2.7	0.282470	7	4.2	−1.4		
	Kattaisenvaara (KV)	KV001	61.4	Perovskite	746	0.511809	7	2.6	0.282448	6	4.1	−1.9	0.702666	17
	Kattaisenvaara (KV)	KV003	33.85	Perovskite	746	0.511829	11	3.0	0.282455	9	4.2	−2.3	0.702683	17
	Lampi	199-07-06	728	Whole-Rock	743	0.511832	13	3.0	0.282459	6	3.8	−2.7		
	Lampi	199-07-06	85	Whole-Rock	743	0.511818	8	2.8	0.282456	8	3.2	−2.9		
	Dike 15	15.4	30.75	Whole-Rock	1,178	0.511150	8	0.7	0.281988	5	−2.5	−5.7		
	Dike 15	15.4	30.67	Whole-Rock	1,178	0.511198	12	1.6	0.281996	4	−2.3	−6.8	0.703383	11
Lentiira-Kuhmo-Kostomuksha	Seitäperä (Kuhmo cluster)	16.12	27.15	Whole-Rock	1,200	0.510700	6	−7.6	0.281710	6	−11.1	−2.9		
	Lentiira (Kuhmo cluster)	LENT W1	-	Whole-Rock	1,203	0.510787	7	−5.8	0.281794	5	−8.1	−2.3		
	Seitäperä (Kuhmo cluster)	6501-B-2	-	Whole-Rock	1,204	0.510764	8	−6.2	0.281728	7	−10.4	−4.0		

Note. $^{143}Nd/^{144}Nd_{CHUR} = 0.512630$; $^{147}Sm/^{144}Nd_{CHUR} = 0.1960$; $^{176}Hf/^{177}HfCHUR = 0.282785$; $^{176}Lu/^{177}Hf_{CHUR} = 0.0336$ from Bouvier et al. (2008).

[a]Initial isotope ratios calculated based on these emplacement ages from Dalton, Giuliani, Phillips, et al. (2020). [b]$\varepsilon Hf_{(i)}$ and $\varepsilon Nd_{(i)}$ is notation for isotope ratios of Nd and Hf, measured in parts per 10 thousand relative to CHUR (CHondritic Uniform Reservoir). [c]$\Delta\varepsilon Hf_{(i)}$ is a measure of displacement of sample $\varepsilon Hf_{(i)}$ from the global mantle Nd-Hf isotope array, at the same sample's $\varepsilon Nd_{(i)}$ value (Vervoort et al., 2011).

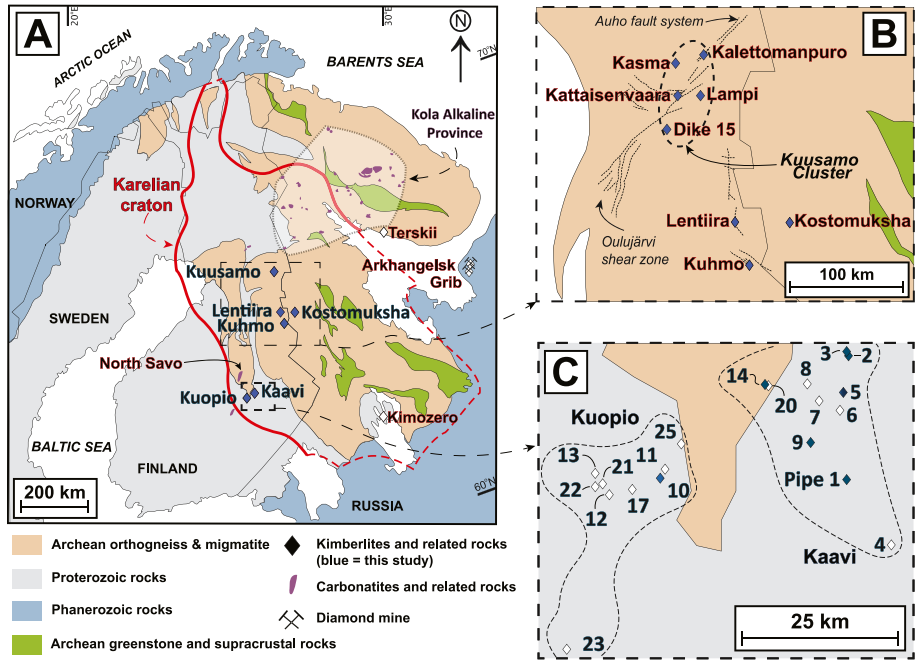

Figure 1. (a) Geological map of the western Fennoscandian Shield. The red outline delimits the boundary of the Karelian Craton; (b) inset, showing the distribution of intrusive bodies in the Kuusamo cluster and the location of Lentiira, Kuhmo and Kostomuksha olivine lamproites; (c) inset showing the distribution of intrusive bodies in the Kaavi-Kuopio kimberlite field, where numbers refer to individual pipe names. In all panels, blue diamonds indicate occurrences sampled for this study. Figure modified from Lehtonen and O'Brien (2009), Nironen (2017) and Dalton, Giuliani, Phillips, et al. (2020).

with intrusions at Kostomuksha (Russia), and were emplaced between ~1,180 and 1,210 Ma (Figure 1; Dalton, Giuliani, Phillips, et al., 2020; O'Brien et al., 2007). Samples from these localities contain abundant phlogopite, lesser olivine macro- and phenocrysts as well as Mn-rich ilmenite, spinel, apatite and perovskite set in a serpentine-phlogopite matrix. Detailed petrographic descriptions for these samples (16.12, LENT-W1 and 6501-B-2) are presented elsewhere (O'Brien, 2015; O'Brien & Tyni, 1999; O'Brien et al., 2007).

At Kuusamo, 100 km to the northeast of Lentiira and Kuhmo (Figure 1), UML dikes were also emplaced in the Mesoproterozoic at 1,180 Ma (Dalton et al., 2019, Dalton, Giuliani, Phillips, et al., 2020), prior to the eruption of seven kimberlites between 735 and 750 Ma, in the same area (Dalton, Giuliani, Phillips, et al., 2020). Given the evolved (i.e., differentiated) nature of the latter, olivine macrocrysts and their psuedomorphs are rare while Ba-rich kinoshitalite mica and perovskite phenocrysts are abundant with lesser apatite, Ti-magnetite and Mg-rich ilmenite in a serpentine-carbonate matrix. The reader is directed to Dalton et al. (2019) for detailed petrographic and geochemical analyses of the samples used in this study.

Some 150 Myr after the emplacement of the Kuusamo kimberlite cluster, 20 kimberlites were emplaced in the Kaavi-Kuopio field of southern Finland, along the edge of the Karelian craton, across a relatively protracted time period between 585 and 620 Ma (Dalton, Giuliani, Phillips, et al., 2020). Samples from Kaavi-Kuopio, while less evolved than those from Kuusamo, display significant petrographic and mineral-chemical variability (Dalton, Giuliani, O'Brien, et al., 2020). They typically contain (sometimes fresh) olivine macro- and microcrysts as well as Cr-rich spinel that exhibits complex zoning through to Ti-magnetite. Further differences from the Kuusamo kimberlites include the relative scarcity and smaller-size of perovskite in these samples and more common Al-poor, Mg-Fe rich phlogopite mica phenocrysts. Mineral and whole-rock geochemical and petrographic assessments of the Kaavi-Kuopio kimberlite samples used here are described in detail in previous work (Dalton, Giuliani, O'Brien, et al., 2020; O'Brien & Tyni, 1999; O'Brien et al., 2005).

3. Methods

All sample preparation and analytical work for this study was carried out at the University of Melbourne.

3.1. Sample Preparation

Rock chips and sections of drill-core, selected based on being the freshest available and a lack of macroscopic xenoliths, were crushed using a steel jaw-crusher. Small chips (<1 cm) representing the freshest, xenolith-free material were hand-picked under a binocular microscope and powdered in a bench top agate ball mill (Retsch Mixer Mill MM 400) for whole-rock isotopic analysis ($n = 16$; Table 1). Perovskite was extracted from additional chips which were crushed using a ring mill, cleaned in distilled water, dried and sieved. A heavy mineral concentrate was prepared from the 25–125 μm size fraction using DIM (diiodomethane) heavy liquid. After cleaning with acetone and drying, the DIM sink fraction was passed over a vertical magnet to remove the highly magnetic fraction, followed by concentration of perovskite on Frantz isodynamic separator (0.6–0.8 A magnetic fraction). Finally, alteration-free euhedral grains from 10 samples were hand-picked under ethanol.

Unleached whole-rock powders were digested with HF-HNO_3 mixtures in Krogh-style polytetrafluorethylene pressure vessels, followed by multiple HCl and HNO_3 treatments to ensure complete dissolution. Perovskite samples were cleaned with dilute nitric acid to remove any adhered carbonate and dissolved at low pressure in Teflon vials on a hotplate at 130°C with a combination of concentrated HF, concentrated HNO_3 and 6M HCl acid. This process produced clear solutions indicative of complete dissolution.

3.2. Column Chemistry and Analytical Procedure

Small (<5%) splits of each solution were reserved for trace element analysis an Agilent 7,700x quadrupole ICP-MS following techniques modified from Kamber et al. (2003).

Larger splits were equilibrated with a ^{149}Sm-^{150}Nd spike for Sm-Nd isotope dilution analyses. In some cases, a ^{176}Lu-^{180}Hf spike was also added. Separation of Sm-Nd was done using Eichrom TRU- and LN-resins (e.g., Pin et al., 2014), while Lu-Hf separations were done using Eichrom LN-resin (modified from Münker et al., 2001). Sr was extracted using Eichrom Sr-resin (e.g., Pin et al., 2014). All isotopic analyses were carried out on a Nu Plasma multi-collector ICP-MS (see Woodhead et al., 2019) Results for $^{143}Nd/^{144}Nd$, $^{176}Hf/^{177}Hf$ and $^{87}Sr/^{86}Sr$ are reported relative to La Jolla = 0.511860, JMC475 = 0.282160 and SRM987 = 0.710230, and have external precisions (2σ) of ±0.000020, ±0.000015 and ± 0.000040, respectively. $^{147}Sm/^{144}Nd$ and $^{176}Lu/^{177}Hf$ ratios from isotope dilution have external precisions (2σ) of ±0.2% and ±1%, respectively, while $^{85}Rb/^{86}Sr$ calculated from trace element concentrations are estimated to have accuracy and precision within ±2%–3% (Woodhead et al., 2019). Results for international standard reference materials (USGS basalts BCR-2 and BHVO-2, Nd solution JNd-1) analyzed with the unknowns are consistent with published values (Table S1 in Supporting Information S1).

4. Results

The initial $^{87}Sr/^{86}Sr$, εNd and εHf compositions for the samples studied here ($n = 24$) are summarized in Table 1. Note that for the kimberlites in the present study, $^{87}Sr/^{86}Sr_{(i)}$ was determined from analysis of perovskite separates rather than whole-rock powders due to anomalously high radiogenic values often associated with whole-rock determination of $^{87}Sr/^{86}Sr_{(i)}$ (e.g., Paton et al., 2007; Woodhead et al., 2009). For the ultramafic lamprophyre from Kuusamo (Dike 15), however, we obtained $^{87}Sr/^{86}Sr_{(i)}$ from the same whole-rock solution used for the Nd and Hf isotope determinations due to the rarity of perovskite in these samples (and considering the freshness of these samples). We also present the first Hf isotopic compositions of kimberlitic perovskites measured by MC-ICP-MS. The only other Hf isotopic study of kimberlitic perovskite was carried out using TIMS analyses (Yang et al., 2009). The full data set, together with existing literature data for these intrusions is presented in Table S1 in Supporting Information S1.

4.1. Lentiira-Kuhmo Olivine Lamproites

The Mesoproterozoic olivine lamproites from Lentiira and Kuhmo preserve a narrow range of sub-chondritic $εNd_{(i)}$ values (−5.8 to −7.6; Table 1; Figure 2), extending the range reported in other studies ($εNd_{(i)}$ −7.0 to −9.4; Figure 2) for olivine lamproites across the 1,180–1,210 Ma Lentiira-Kuhmo-Kostomuksha cluster (Kargin et al., 2014; O'Brien & Tyni, 1999). The $εHf_{(i)}$ values, the first Hf isotope data for olivine lamproites in this region, are also sub-chondritic, range from −8.1 to −11.1 and plot just below the mantle array ($ΔεHf_{(i)}$ −2.3 to

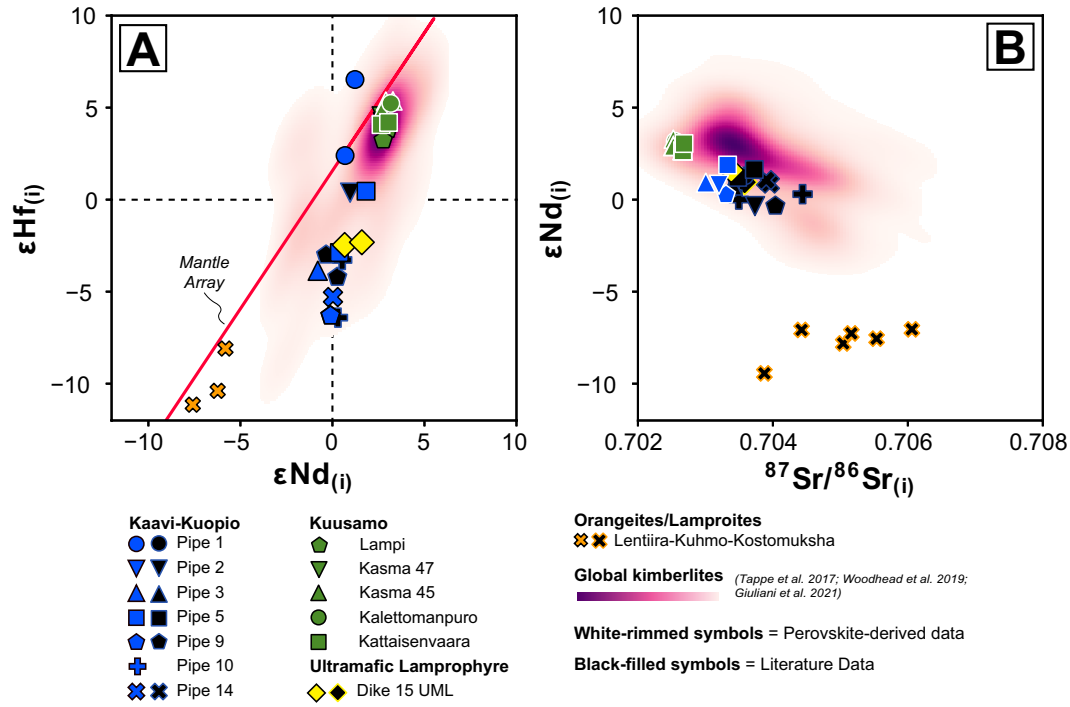

Figure 2. Bivariate plots of initial Sr-Nd-Hf isotope compositions for kimberlites and related rocks in Finland. (a) $\varepsilon Hf_{(i)}$ versus $\varepsilon Nd_{(i)}$; (b) $\varepsilon Nd_{(i)}$ versus $^{87}Sr/^{86}Sr_{(i)}$. Symbols with white rims represent perovskite, all other symbols represent whole rock compositions. Existing literature data (black-filled symbols) for these occurrences from Kargin et al. (2014); O'Brien and Tyni (1999); Woodhead et al. (2019), see Table S1 in Supporting Information S1 for details. For comparison, global kimberlite compositions are also shown (see Giuliani et al., 2021; Tappe, Romer, et al., 2017; Woodhead et al., 2019), with dominant compositions highlighted using a kernel density estimate tool (pyrolite Python module, Williams et al., 2020). Mantle array from Veervort et al. (2011).

−4.0) of Vervoort et al. (2011). This is consistent with Nd-Hf isotope data for similar rock types (orangeites) in southern Africa (e.g., Coe et al., 2008; Nowell et al., 2004).

4.2. Kuusamo Kimberlites and Ultramafic Lamprophyres

The ~750 Ma Kuusamo kimberlites display a very limited range of supra-chondritic $\varepsilon Nd_{(i)}$ values (+2.7 to +3.3; Table 1; Figure 2), regardless of whether these data are extracted from whole-rock (Lampi and Kasma 47 only) or perovskite analyses. Corresponding $\varepsilon Hf_{(i)}$ values range from +3.2 (Lampi) to + 5.4 (Kasma 45, Table 1; Figure 2). It is notable that the Kuusamo kimberlites plot in the high-density compositional zone of global kimberlites in $\varepsilon Nd_{(i)}$-$\varepsilon Hf_{(i)}$ space as shown in Figure 2 and only slightly below the mantle array ($\Delta\varepsilon Hf_{(i)}$ −0.97–−2.9). Perovskite-derived $^{87}Sr/^{86}Sr_{(i)}$ is similarly homogenous (0.70252–0.70268; Table 1; Figure 2); a trend to lower $^{87}Sr/^{86}Sr_{(i)}$ than compositions recorded in global kimberlites may not be representative as published $^{87}Sr/^{86}Sr_{(i)}$ values are based mostly on Cretaceous samples. The average radiogenic isotope composition for Dike 15, the Mesoproterozoic ultramafic lamprophyre (aillikite), plots in between the contemporaneous Lentiira-Kuhmo-Kostomuksha olivine lamproites and Neoproterozoic Kuusamo kimberlites ($\varepsilon Hf_{(i)} = -2.4 \pm 0.1$; $\varepsilon Nd_{(i)} = +1.1 \pm 0.4$; $^{87}Sr/^{86}Sr_{(i)} = 0.70348 \pm 10$; Table 1; Figure 2) and hence further below the Nd-Hf mantle array ($\Delta\varepsilon Hf_{(i)}$ −6.3 ± 0.6) compared to the Kuusamo kimberlites.

4.3. Kaavi-Kuopio Kimberlites

Whole-rock and perovskite $\varepsilon Nd_{(i)}$ values for the ~600 Ma Kaavi-Kuopio kimberlites are slightly less geochemically depleted than those for Kuusamo but span a greater range (−0.8 to +2.0; Table 1; Figure 2) and marginally increase the range of published whole-rock values (−0.4 to +1.6; O'Brien & Tyni, 1999; Peltonen et al., 1999; Woodhead et al., 2019). We note that perovskite and whole-rock $\varepsilon Nd_{(i)}$ values for some samples reported here

are indistinguishable (samples 2.151, 3.96 and 5.7; Table 1), whereas the perovskite $\varepsilon Nd_{(i)}$ value for sample 9.2 is higher than in the whole-rock (+2.0 vs. −0.2). Such a variation may be related to the degree of alteration in whole-rock samples relative to perovskite separates. Pipe 9 samples display evidence of alteration/crustal contamination (Dalton, Giuliani, O'Brien, et al., 2020) which may modify whole-rock Nd isotopic compositions to a greater extent relative to perovskite grains. Relative to the global kimberlite database, it is notable that the Kaavi-Kuopio samples are closer to chondritic compositions.

Perovskite-derived initial $^{87}Sr/^{86}Sr_{(i)}$ ratios for Pipe 2, 3, 5 and 9 have a limited range (0.70300–0.70333). In every instance, these values are less radiogenic than published whole-rock values from the same pipe (0.70340–0.70404; recalculated using updated decay constant of Villa et al., 2015). This observation is consistent with previous comparisons of perovskite and whole-rock $^{87}Sr/^{86}Sr_{(i)}$ values and the susceptibility of the latter to disturbance by even minor crustal contamination (e.g., Paton et al., 2007; Pearson et al., 2019; Woodhead et al., 2009).

A significant feature of the Kaavi-Kuopio kimberlite samples is the large range in $\varepsilon Hf_{(i)}$ compositions, spanning over 12 epsilon units (+6.5 to −6.3). Published $\varepsilon Hf_{(i)}$ values for Pipe 2, 9 and 10 range from +0.4 to −6.4 (Woodhead et al., 2019), while it is notable that Pipe 1 values vary by 4 $\varepsilon Hf_{(i)}$ units. Such variation may be due to differences in sample freshness, lithospheric and/or crustal contamination or mantle source variability, though it is difficult to identify which, if any of these factors may be the cause. Together, these data form a near-vertical linear distribution in $\varepsilon Nd_{(i)}$-$\varepsilon Hf_{(i)}$ space which extends to $\varepsilon Hf_{(i)}$ values far lower than is typical of kimberlites elsewhere and lies at a very steep angle to the mantle array. This dispersion from the mantle array is highlighted by $\Delta\varepsilon Hf_{(i)}$ values which range from +2.5 to −9.1. Such extreme displacement is rare for kimberlites globally, but has been observed in Mesozoic samples from Lac de Gras, Canada ($\Delta\varepsilon Hf_{(i)} = -6.6$ to +9.8; Tappe et al., 2013) and Tikiusaaq, West Greenland ($\Delta\varepsilon Hf_{(i)} = -6.6$ to +9.8; Tappe, Romer, et al., 2017).

5. Discussion

5.1. Geodynamic and Source Constraints for ~1,200 Ma Olivine Lamproite and Ultramafic Lamprophyre Magmatism in Eastern Finland

Olivine lamproites were intruded into the Karelian craton over a protracted period from ~1,210 to 1,180 Ma at Lentiira, Kuhmo and Kostomuksha (Dalton, Giuliani, Phillips, et al., 2020; O'Brien et al., 2007). The youngest members of this cluster overlap temporally with the emplacement of the Kuusamo UMLs (aillikites; 1,178 ± 5 Ma; Dalton et al., 2019) 100 km to the northwest (Figure 1).

The paleoposition and tectonic regime of Baltica at this point in time is somewhat uncertain. Coeval mafic dike swarms suggest that Baltica and Laurentia were united until ca. 1.25 Ga (Mertanen & Pesonen, 2005). At this stage extensional tectonics dominated, potentially culminating in the separation of Baltica from Laurentia at ~1.2 Ga (e.g., Bingen et al., 2002; Bogdanova et al., 2008). In contrast, the interpretation of paleomagnetic evidence led Salminen et al. (2009) to suggest a longer-lived Baltica-Laurentia relationship, until ~1.12 Ga. The presence of an extensional regime between ~1.27 and 1.20 Ga (or potentially 1.12 Ga) is consistent with episodic mantle-derived igneous activity in Sweden and Finland (Bogdanova et al., 2008 and references therein), including the Central Scandinavian Dolerite Group.

The ~1.2 Ga extensional regime may have facilitated local upwelling of asthenospheric material, which partially melted to generate the Kuusamo UMLs. It is also notable that the Baltica examples are synchronous with ultramafic alkaline magmatism (olivine lamproites and UMLs) which intruded the Greenland portion of the North Atlantic craton (part of Laurentia) in the Mesoproterozoic (e.g., Larsen & Rex, 1992; Nelson, 1989; Secher et al., 2009; Upton et al., 2003). Therefore, it is plausible that these occurrences also resulted from the extensional regime that prevailed in the Laurentia-Baltica continental block.

Dalton et al. (2019) proposed that the aillikites (e.g., Dike 15) at Kuusamo represent asthenosphere-derived melts that have had minor interaction with metasomatized SCLM whereas the olivine lamproites are the result of extensive interaction between these asthenospheric melts and the SCLM. The new Nd-Hf isotopic data for the Lentiira-Kuhmo samples presented in this study ($\varepsilon Nd_{(i)}$ −5.8 to −7.6; $\varepsilon Hf_{(i)}$ −8.1 to −11.1; Figure 2) are consistent with an origin for this cluster of olivine lamproites in metasomatically enriched SCLM. This scenario was also proposed for the genesis of the neighboring Kostomuksha olivine lamproites by Kargin et al. (2014) and has often

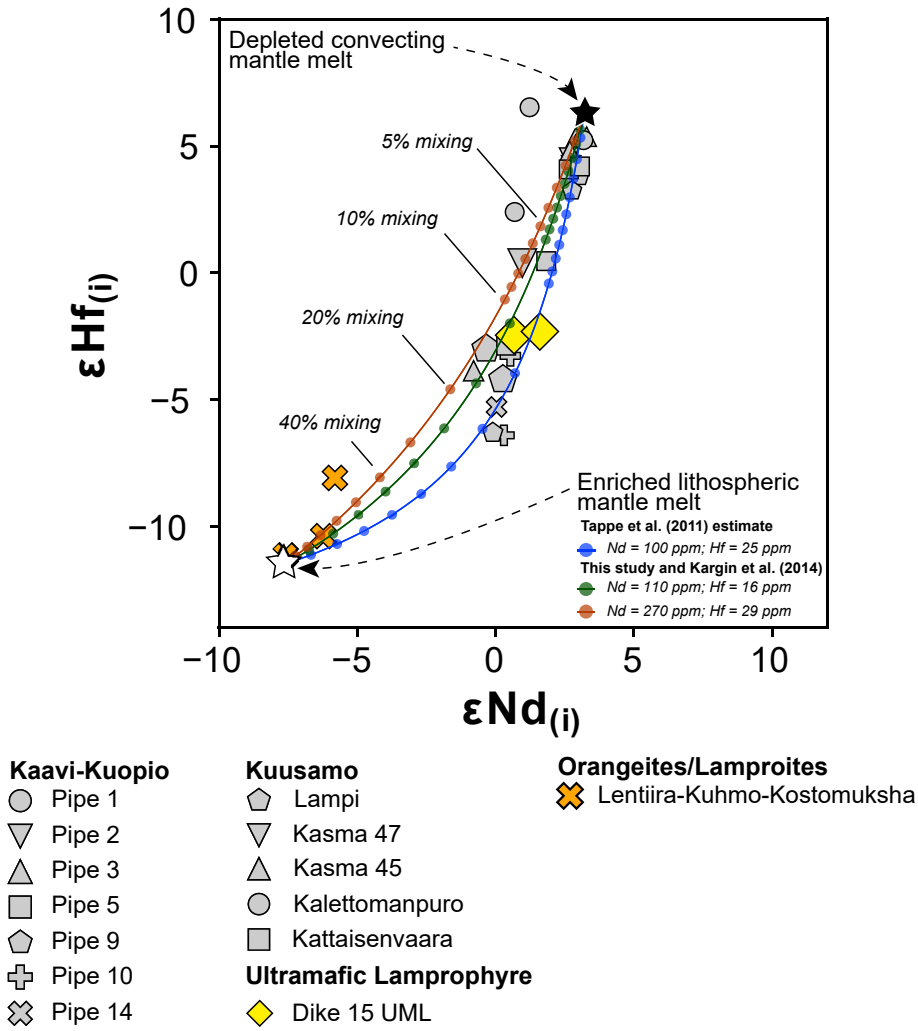

Figure 3. Bivariate plot of $^{176}Hf/^{177}Hf_{(i)}$ versus $^{143}Nd/^{144}Nd_{(i)}$ for kimberlites and related rocks from Finland, with emphasis on the ultramafic lamprophyres and olivine lamproites. Binary mixing relationships are shown between a geochemically depleted asthenospheric melt similar to the PREvalent MAntle component of Giuliani et al. (2021) and a melt sourced within the enriched subcontinental mantle lithosphere - composition from Tappe et al. (2011) and this work (see text). Mixing approximately 15%–20% of a melt phase from enriched subcontinental lithospheric mantle to the asthenospheric melt reproduces the isotopic composition of Dike 15 ultramafic lamprophyre. See Table S2 in Supporting Information S1 for full model parameters.

been suggested for cratonic lamproites globally (e.g., Coe et al., 2008; Fitzpayne et al., 2018; Fraser et al., 1985; Giuliani et al., 2015; Pandey & Rao, 2020).

Relative to olivine lamproites, the aillikite samples from Dike 15, have more radiogenic Nd-Hf compositions ($\varepsilon Hf_{(i)} = -2.4 \pm 0.1$; $\varepsilon Nd_{(i)} = +1.1 \pm 0.4$; Figure 2) and plot below the values typical of global kimberlites. Indeed, Dike 15 Nd-Hf isotope compositions lie intermediate between the composition of kimberlites and those of the olivine lamproites (Figure 3). This intermediate composition suggests that Dike 15 is not a melt produced solely from the convecting mantle. As suggested in Dalton et al. (2019), this isotopic signature may instead reflect interaction of Dike 15 parental melts with metasomatized components in the SCLM during magma transport to surface. This model is also consistent with petrogenetic models put forward by Tappe et al. (2008) for aillikites whereby UMLs exist on a continuum between olivine lamproites and carbonate-rich melts which may derive from the asthenosphere. In this hypothesis the convective mantle-derived magma interacts with a K-rich melt within the metasomatized cratonic lithosphere to induce the UML-like characteristics. In the present study, a caveat to this continuum model is that the proto-aillikite magma interacted with a lesser proportion of the

same or similar metasomatized SCLM component that dominates the proposed source of the olivine lamproites, despite being separated by ~100 km. In this regard, a geothermobarometric study of garnet and clinopyroxene xenocrysts from kimberlites and olivine lamproites (Lehtonen & O'Brien, 2009), suggests that the lithospheric mantle beneath Kuusamo, is indeed similar to that beneath the Lentiira-Kuhmo cluster.

Before testing this scenario quantitatively, we first rule out the possibility of bulk assimilation of incompatible element-enriched lithology akin to MARID (mica-amphibole-rutile-ilmenite-diopside xenolith)-like compositions (Fitzpayne et al., 2018, 2019; Grégoire et al., 2002). Involvement of such lithologies can cause potentially extreme shifts in $^{176}Hf/^{177}Hf$ without disturbing $^{143}Nd/^{144}Nd$ to the same extent (e.g., Choukroun et al., 2005; Fitzpayne et al., 2019; Tappe et al., 2011). For the convecting melt end-member, we employ the geochemically depleted PREMA (PREvalent MAntle; Zindler & Hart, 1986) source component of Giuliani et al. (2021), corrected to 1,200 Ma, which is considered to be a ubiquitous source component of kimberlites and carbonate-rich UMLs globally and therefore a reasonable proxy for this starting composition. Binary mixing models utilizing age-corrected isotope compositions of southern African MARID from Fitzpayne et al. (2019) cannot produce Nd-Hf isotopic shifts that replicate the observed compositional range of the Kuusamo aillikites (Figure S1 in Supporting Information S1; model parameters in Table S2 in Supporting Information S1). Therefore, we also employed the isotopic compositions of the lamproites as proxies of the local metasomatized SCLM. Based on this modeling it appears that an unrealistic proportion (i.e., >50%) of enriched SCLM material would need to be incorporated into the ascending melt to cause a meaningful shift in Nd-Hf isotope compositions (Figure S2 in Supporting Information S1; model parameters in Table S2 in Supporting Information S1).

With bulk assimilation a seemingly unlikely cause of isotopic enrichment, we instead follow the approach of Tappe et al. (2008, 2011) and model the isotopic composition of an UML magma that is generated by mixing the same PREMA-derived melt used in the assimilation model above with a component derived by melting an enriched metasome in the SCLM. For this latter enriched end member, we utilize the Nd-Hf elemental and isotopic compositions of the Lentiira-Kuhmo-Kostomuksha lamproites as well as an Nd and Hf lamproite-like concentrations of Tappe et al. (2011), for comparative purposes. The results of this model vary based on the Nd/Hf of the enriched melt component, however, mixing of just ~15%–20% of an enriched melt component is required to generate $\varepsilon Nd_{(i)}$-$\varepsilon Hf_{(i)}$ compositions consistent with those of the Dike 15 aillikite magma, in line with the proportions proposed by Tappe et al. (2008, 2011) for similar UMLs from the North Atlantic craton.

5.2. Origin of ~750 Ma Kimberlite Magmatism at Kuusamo

The Kuusamo kimberlites were emplaced between ~730 and 750 Ma (Dalton, Giuliani, Phillips, et al., 2020). Again, there is some uncertainty regarding the tectonic setting of Baltica at this time (e.g., Cawood & Pisarevsky, 2006; Hartz & Torsvik, 2002). Baltica formed part of the Rodinia supercontinent up to ~750 Ma when break-up of Rodinia began (e.g., Johansson, 2014; Li et al., 2008; Merdith et al., 2017; Merdith et al., 2021). It has been suggested that the Kuusamo kimberlites were emplaced along Precambrian shear-zones (Dalton et al., 2019) and it is possible that far-field stresses related to supercontinent break-up reactivated these older structures hence facilitating the ascent of kimberlitic magmas to surface. A similar scenario has been proposed for kimberlite magmatism in other regions worldwide (e.g., Bailey & Lupulescu, 2015; Chalapathi Rao et al., 2017; Jelsma et al., 2009; Moore et al., 2008; Parrish & Lavin, 1982; Tappe et al., 2014).

As an alternative, proximity to the "superplume" that is believed to trigger the onset of Rodinia break-up (e.g., Li et al., 2008; Robert et al., 2021) may have provided the requisite impetus for mantle melting and kimberlite genesis. It has been suggested that Baltica was situated peripheral to a modeled superplume (Li et al., 2008) located at the margin of a LLSVP (assuming temporal fixity of these lower mantle structures; Torsvik, 2019, Figure 4). Based on this peripheral position it is anticipated that the heat flux and, therefore, degree of melting associated with this anomaly would be relatively low, consistent with the production of carbonated silicate melts such as kimberlites (e.g., Ernst et al., 2019).

Importantly, based on the paleogeographic evidence available, we can likely rule out the role of subduction or other collisional events as being the geodynamic trigger for kimberlite magmatism at this time. It has been tentatively suggested that subduction may have occurred outboard of Baltica at around 800 Ma (e.g., Merdith et al., 2017; Merdith et al., 2021). However, there is no evidence for inboard subduction contemporaneous with the Kuusamo or younger Kaavi-Kuopio kimberlites (discussed below) which is at odds with examples of

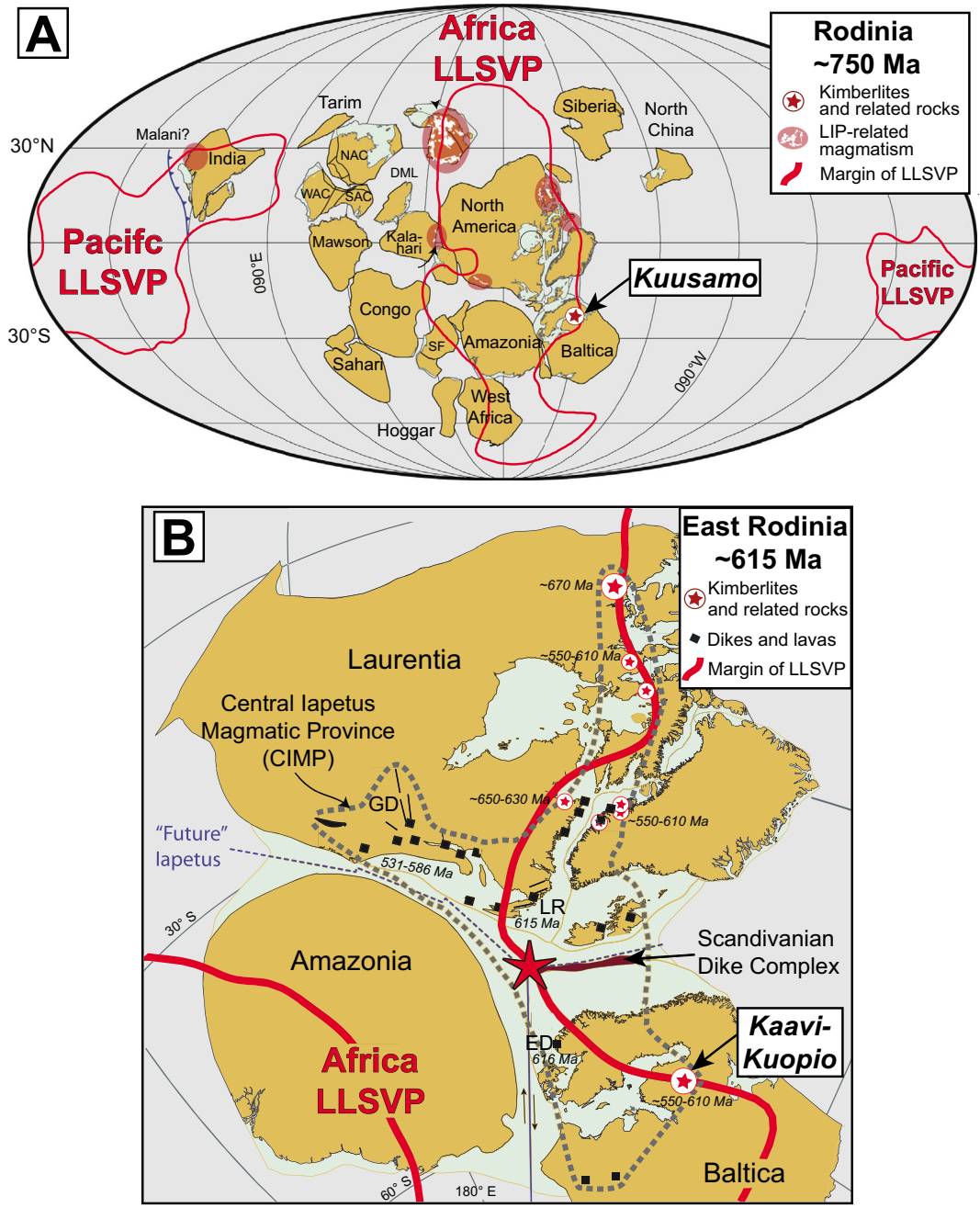

Figure 4. (a) Rodinia reconstruction at ~750 Ma showing the present-day position of the "Africa" and "Pacific" Large Low Shear-wave Velocity Provinces (LLSVP's; diagram modified from Torsvik, 2019). Note the position of the Kuusamo kimberlite cluster at the margin of the Africa LLSVP. (b) Reconstruction of East Rodinia at ~615 Ma. Note the position of the Kaavi-Kuopio kimberlite localities on the margins of both the African LLSVP and Central Iapetus Magmatic Province (CIMP; gray dotted line), as defined by Tegner et al. (2019). Also shown are mafic dike swarms within the CIMP (Scandinavian Dike Complex, GD = Grenville Dike Complex, LR = Long Range Dike Complex, ED = Egersund Dike Complex), and kimberlites and related rocks that temporally overlap with the Kaavi-Kuopio kimberlites. Large red star indicates the suggested location of the mantle plume head which generated the CIMP. Diagram modified from Tegner et al. (2019).

kimberlites from North America where subduction is thought to have played some role in their genesis (e.g., Currie & Beaumont, 2011; Duke et al., 2014; Kjarsgaard et al., 2017).

In terms of isotopic composition, the source of the Kuusamo kimberlites appears indistinguishable from compositions that are considered "typical" of kimberlites globally (Figure 2); that is, a moderately depleted reservoir that extends from marginally supra-chondritic PREMA-like Nd-Hf(-Sr) isotope compositions to near-chondritic values (see Giuliani et al., 2021). In this sense, the Kuusamo kimberlites also appear to represent pristine samples of the ancient kimberlite source hypothesized by Woodhead et al. (2019). A final, remarkable feature of the isotope systematics of the Kuusamo kimberlites is their stark contrast with the Kaavi-Kuopio kimberlites, which are discussed below.

5.3. Geodynamic and Source Constraints for the ~600 Ma Kaavi-Kuopio Kimberlites

Whereas the Kuusamo kimberlites record the first stage of Rodinia break-up, the ~585–620 Ma Kaavi-Kuopio kimberlites are contemporaneous with the final stages of supercontinent disintegration and the opening of the Iapetus ocean that separated Laurentia from Baltica. The initial phase of the Iapetus opening is linked to the emplacement of the Central Iapetus Magmatic Province (CIMP; Figure 4), a composite large igneous province (LIP) that includes mafic as well as alkali- and volatile-rich mantle-derived magmas (e.g., Ernst & Bell, 2010; Grant et al., 2020). While longer-lived and volumetrically insignificant compared to LIPs associated with flood basalt magmatism, the CIMP is still attributed to a mantle plume(s) origin (e.g., Ernst & Bell, 2010; Puffer, 2002; Robert et al., 2021; Tegner et al., 2019; Weber et al., 2019), which might have stemmed from the margin of the African LLSVP (Figure 4; Murphy et al., 2021; Tegner et al., 2019). The first pulse of this LIP is well constrained at ~615 Ma based on the dating of three dike swarms (Egersund, Long Range and Novillo) from Baltica, Laurentia and Amazonia (Bingen et al., 1998; Kamo et al., 1989; Weber et al., 2019). At least an additional two further pulses of magmatic activity at ~590 Ma and ~560–570 Ma are associated with the CIMP, with complete opening of the Iapetus ocean achieved by ~540 Ma (e.g., Cawood et al., 2001; Ernst, 2014; Ernst & Bell, 2010; Merdith et al., 2017; Merdith et al., 2021; Robert et al., 2020).

It is notable that this period of Neoproterozoic magmatism also includes the emplacement of kimberlites, UMLs and carbonatites in areas of former Rodinia that were contiguous with Baltica (Figure 4), that is, Norway (Fen and Alnö; ~580–590 Ma); West Greenland (Manitsoq, Sarfartoq; ~550–610 Ma) and eastern North America (Amon, Renard, Aillik Bay, Torngat; ~580–670 Ma) (e.g., Doig, 1970; Larsen & Rex, 1992; Meert et al., 2007; Ranger et al., 2018; Rukhlov & Bell, 2010; Tappe et al., 2011; Tappe, Brand, et al., 2017). This activity has similarly been linked to the supercontinent break-up and opening of the Iapetus ocean and/or the related impact of one or multiple mantle plumes (e.g., Ernst, 2014; Heaman et al., 2004; Tappe et al., 2014; Tappe, Brand, et al., 2017). We envisage a similar scenario for the genesis of the Kaavi-Kuopio kimberlites; that is, magma genesis as a result of the spatiotemporal overlap between deep-mantle upwellings and lithospheric extension associated with supercontinent breakup.

Though both kimberlite occurrences in Finland are hypothesized to be linked to mantle plumes associated with the demise of Rodinia, the >100 Myr between the cessation of kimberlite activity at Kuusamo and initiation of magmatism at Kaavi-Kuopio provided ample time for variations in the composition, thermal properties and hence melting regime of the convective mantle sources of these kimberlites. In fact, Baltica migrated anywhere between ~1,000 km (Robert et al., 2021) and ~5,000 km (Merdith et al., 2021) between ~750 Ma and ~600 Ma. The Hf isotopic compositions of the Kaavi-Kuopio kimberlites are strikingly heterogeneous relative to the more tightly clustered isotopic compositions of the Kuusamo kimberlites (Figure 2). If the latter represent the "archetypal" case of kimberlite derivation from partial melting of a deep and potentially ancient mantle source (Giuliani et al., 2021; Nakanishi et al., 2021; Woodhead et al., 2019), then the Kaavi-Kuopio kimberlites may reflect genesis from a more heterogeneous source under potentially more complex geodynamic circumstances. An additional complexity to consider is the role of a heterogeneous mantle lithosphere, particularly variations in lithospheric thickness, because kimberlites are well known to extensively interact with and assimilate lithospheric mantle material (e.g., Giuliani et al., 2020b; Russell et al., 2012; Soltys et al., 2016; Tovey et al., 2021; Xu et al., 2021). The latter has been shown to have a pivotal role in the major element make-up of primitive melts parental to the Kaavi-Kuopio kimberlites (Dalton, Giuliani, O'Brien, et al., 2020).

5.3.1. Geothermobarometric Effects

If kimberlite melts are generated by partial melting at or just below the LAB, spatial heterogeneities in lithospheric thickness could have influenced the extent of partial melting (e.g., Gudfinnsson & Presnall, 2005; Massuyeau et al., 2021) and hence the composition of kimberlite magmas including Hf isotope variability in the Kaavi-Kuopio region. In this scenario we envisage that changes in the LAB depth, possibly due to thermal erosion or extensional tectonics during the ~30 Myr of kimberlite activity, would have influenced the degree of melting (lower for deeper LAB), with lower degree melts preferentially sampling more enriched, more fusible portions of the same sub-lithospheric source (e.g., Ito & Mahoney, 2005a; Ito & Mahoney, 2005b; Stracke, 2021) thus generating kimberlites with lower $\varepsilon Hf_{(i)}$.

We utilized both kimberlite-entrained xenocryst geothermobarometry (Mather et al., 2011; Nimis & Taylor, 2000) and olivine-chromite geothermometry (Ballhaus et al., 1994; Fedortchouk & Canil, 2004; O'Neill & Wall, 1987) to assess the impact of any geothermobarometric effects on the isotopic composition of the Kaavi-Kuopio kimberlites. The quantitative models reported in Text S1 in Supporting Information S1 and Figures S3-S4 in Supporting Information S1) indicate that neither variations in lithospheric thickness nor melt and hence source temperature can account for the observed variations in $\varepsilon Hf_{(i)}$ composition.

5.3.2. The Role of Lithospheric Assimilation

Though it is recognised that mantle assimilation alters major element compositions of kimberlitic melts (e.g., Dalton, Giuliani, O'Brien, et al., 2020; Giuliani et al., 2020a; Xu et al., 2021), it remains to be seen if this same process can account for variations in incompatible trace elements and hence the Hf isotope variations in the Kaavi-Kuopio kimberlites. In support of this hypothesis are the statistically significant correlations observed between bulk-rock or perovskite $\varepsilon Hf_{(i)}$ and the Mg# of olivine xenocryst cores (proxy for assimilated mantle material; $R^2 = 0.94$, $p = 0.03$) as well as various proxies for primitive melt composition, such as olivine rim Mg# ($R^2 = 0.92$, $p = 0.04$) and chromite Mg# ($R^2 = 0.67$, $p = 0.03$) and chromite TiO_2 contents ($R^2 = 0.71$, $p = 0.02$; Figure 5). The relationships in samples that preserve fresh olivine as well as chromite ($n = 4$) are robust, making it possible to assess the influence of assimilation in samples lacking fresh olivine based on the Mg# and TiO_2 contents of chromite grains alone ($n = 7$; Figures 5c and 5d).

Previous attempts to unravel the effect of mantle assimilation on kimberlite isotopic compositions using mass balance constraints showed that unrealistically high levels of assimilation (20%–90%) were required to displace Nd-Hf isotopic compositions of Lac de Gras kimberlites (Canada) from the mantle array (Tappe et al., 2013; Tovey et al., 2021). Recent work on the Premier kimberlite also showed no relationship between Nd-Hf isotope decoupling and assimilation of mantle material (Tappe, Stracke, et al., 2020). These models are more difficult to replicate for the Finnish kimberlites because, unlike the Slave or Kaapvaal cratons, the isotopic composition of the Karelian craton SCLM is poorly constrained. Peltonen et al. (1999) presented Sr-Nd isotope data (whole rocks, mineral separates) for mantle xenoliths entrained by the Kaavi-Kuopio kimberlites which overlap closely with the Sr-Nd isotope compositions of the kimberlites (Figure S5 in Supporting Information S1. It was noted by Peltonen et al. (1999) that this isotopic similarity may be linked to recent kimberlite metasomatism of the lithospheric mantle as also noted for mantle xenoliths in the Kimberley area (South Africa - e.g., Fitzpayne et al., 2019, 2020; Grégoire et al., 2002).

If kimberlite or proto-kimberlite metasomatism largely influenced the isotopic composition of the lithospheric mantle that was entrained and assimilated, it is improbable, based on compositional and mass balance constraints, that lithospheric mantle assimilation generated the significant heterogeneity observed in $\varepsilon Hf_{(i)}$ compositions of the Kaavi-Kuopio kimberlites (+4.5–−5.3). An additional nuance is that the Karelian lithospheric mantle beneath Kaavi-Kuopio appears to have become more enriched (on the basis of decreasing olivine xenocryst core Mg#) during the ~35 Myr of kimberlite emplacement ($R^2 = 0.95$, $p = 0.03$; Figure 6), which implies that continued pulses of kimberlitic melts *progressively* modified the lithosphere. Similar modifications of the SCLM by earlier pulses of kimberlite magmas has been widely recognised in the Kimberley area (South Africa - e.g., Dawson et al., 2001; Fitzpayne et al., 2019; Fitzpayne et al., 2020; Giuliani et al., 2013; Giuliani et al., 2014; Giuliani et al., 2016; Konzett et al., 1998). It then follows that the source region of these metasomatic agents (i.e., proto-kimberlites) may also have undergone progressive isotopic enrichment. If mantle assimilation was the driver of the variations in $\varepsilon Hf_{(i)}$ compositions, one would expect the oldest kimberlite to show the most enriched isotopic signatures (i.e., lowest $\varepsilon Hf_{(i)}$) as these intrusions would readily assimilate the most enriched and therefore

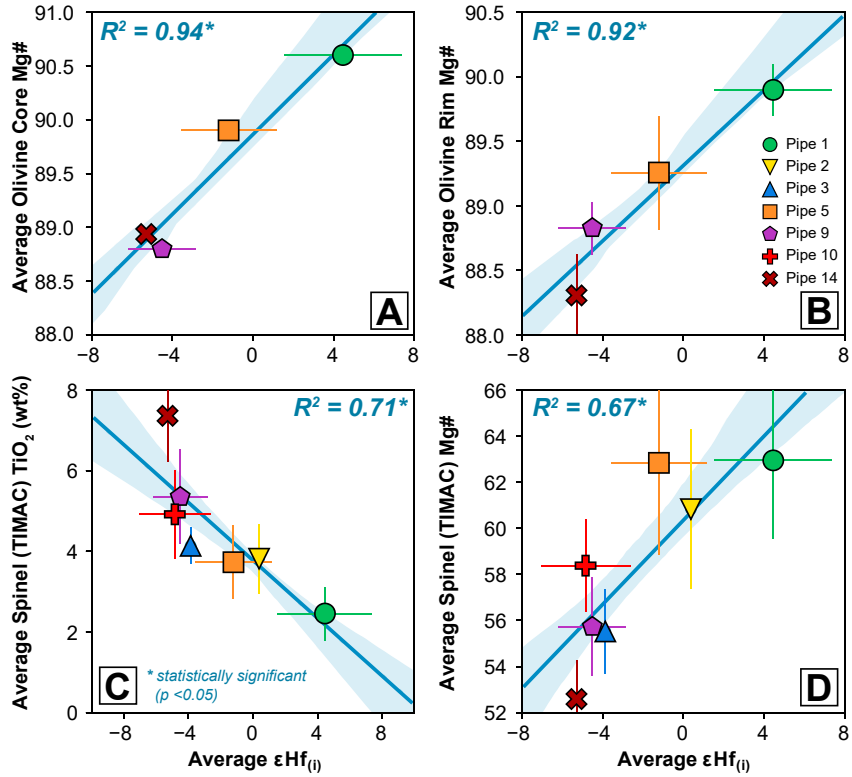

Figure 5. Relationship between average $\varepsilon Hf_{(i)}$ (of bulk rocks and perovskites) and olivine and spinel compositions for the Kaavi-Kuopio kimberlites. (a) Average olivine core Mg# versus average $\varepsilon Hf_{(i)}$; (b) Average olivine rim Mg# versus average $\varepsilon Hf_{(i)}$; (c) Average chromite TiO_2 content versus average $\varepsilon Hf_{(i)}$; (d) Average chromite Mg# versus average $\varepsilon Hf_{(i)}$. Mineral composition data from Dalton, Giuliani, O'Brien, et al. (2020). R^2 is the correlation coefficient of the linear regressions, shaded field represents a 1 standard deviation uncertainty envelope. Statistical significance determined using linear regression analysis in the Minitab 20 software package.

most fusible lithospheric mantle material. Indeed, Tovey et al. (2021) observed this pattern in the isotopic signatures for the Lac de Gras kimberlites where the youngest kimberlites yield the most depleted $^{176}Hf/^{177}Hf_{(i)}$ compositions. However, in the present study the opposite pattern is observed whereby kimberlite $\varepsilon Hf_{(i)}$ compositions shift toward lower $\varepsilon Hf_{(i)}$ values with decreasing age of emplacement ($R^2 = 0.72$, $p = 0.02$; Figure 6).

Additional evidence against the role of assimilation in displacing Hf compositions may lie in the robust relationship ($R^2 = 0.67$, $p = 0.02$; Figure 7) between oxygen fugacity (fO_2) values presented by Dalton, Giuliani, O'Brien, et al. (2020) and our new $\varepsilon Hf_{(i)}$ data, whereby more enriched Hf isotope signatures (i.e., negative $\varepsilon Hf_{(i)}$) are linked to more reduced fO_2 values (i.e., negative ΔNNO). We note that Pipe 14 has a poorly constrained fO_2 (-2.3 ± 3.3); removing this data point only strengthens the observed relationship ($R^2 = 0.82$, $p = 0.01$). Although there are some limitations associated with the perovskite and monticellite oxybarometers (Bellis & Canil, 2007; Canil & Bellis, 2007; Le Pioufle and Canil, 2012), the relative differences in fO_2 rather than absolute values are of importance here. Metasomatized mantle lithosphere is considered to be oxidized (e.g., Foley & Fischer, 2017; Foley et al., 2019; Woodland et al., 1996; Yaxley et al., 2017). Therefore it follows, to a first order approximation, that progressive assimilation of enriched SCLM material increases oxidation levels in kimberlite melts. The current data show the opposite pattern, suggesting that assimilation of metasomatized lithospheric mantle cannot explain the spread in Hf isotope compositions. Further below, we explore the possibility that these fO_2 variations are a function of variability in the kimberlite source composition.

In summary, it is apparent that mantle assimilation played only a minor, if any, role in causing the observed changes in Hf isotopic compositions. Therefore, the role of temporal source evolution is now considered.

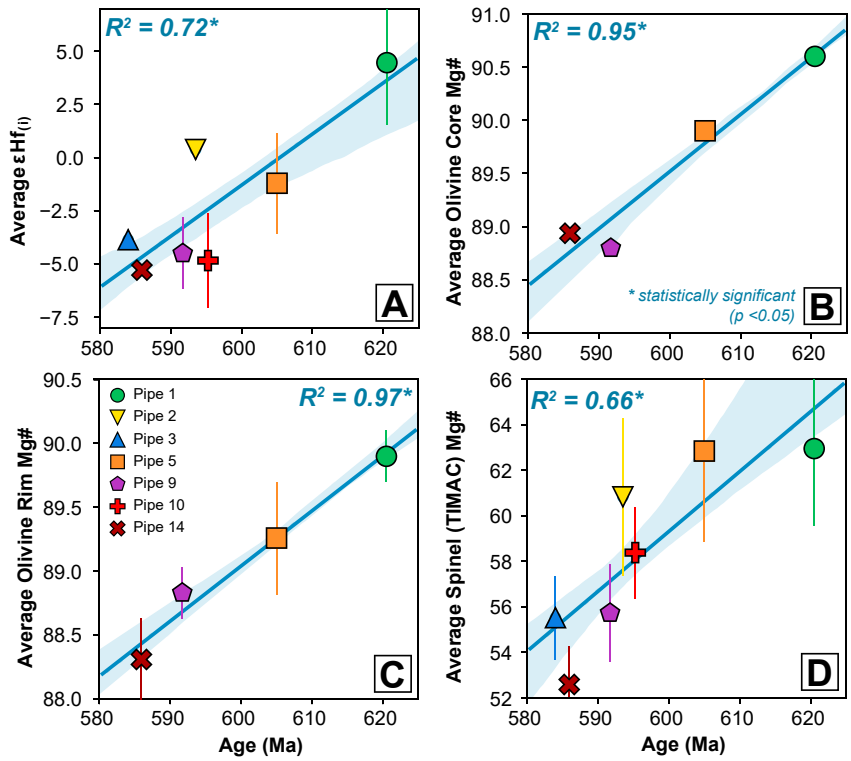

Figure 6. Relationship between emplacement age and, $\varepsilon Hf_{(i)}$, olivine and spinel compositions with linear regression models fitted for the Kaavi-Kuopio kimberlites. (a) Age versus average $\varepsilon Hf_{(i)}$; (b) Age versus. average olivine core Mg#; (c) Age versus. average olivine rim Mg#; (d) Age versus average chromite Mg#. Mineral composition data from Dalton, Giuliani, O'Brien, et al. (2020), age data from Dalton, Giuliani, Phillips, et al. (2020). R^2 is the correlation coefficient, shaded field represents a 1 standard deviation uncertainty envelope. Statistical significance determined using linear regression analysis in the Minitab 20 software package.

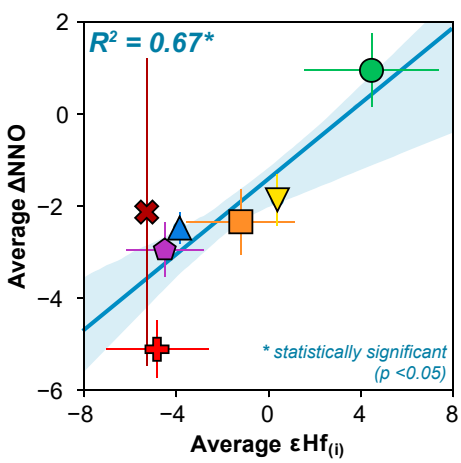

Figure 7. Linear relationship between $\varepsilon Hf_{(i)}$ and oxygen fugacity (displayed as ΔNNO) in the Kaavi-Kuopio kimberlites. Oxygen fugacity data calculated using perovskite and monticellite compositions are from Dalton, Giuliani, O'Brien, et al. (2020). R^2 is the correlation coefficient, shaded field represents a 1 standard deviation uncertainty envelope. Statistical significance determined using linear regression analysis in the Minitab 20 software package. Symbols as per Figure 5.

5.3.3. Progressive Enrichment of the Kimberlite Source Region

With variations in lithospheric thickness and mantle assimilation both apparently unlikely causes of isotopic variation, we now must consider causes of local source heterogeneity. It has been argued (e.g., Fitzpayne et al., 2021; Giuliani et al., 2021; Nakanishi et al., 2021; Nowell et al., 2004; Tappe, Stracke, et al., 2020, 2013; Woodhead et al., 2019) that subducted material may be an important source contaminant for post-Mesozoic kimberlites, but it is unclear whether or not this process had any role in older kimberlites as suggested by Tappe, Budde, et al. (2020) for the Mesoproterzoic Premier kimberlite in South Africa. Here, we investigate whether recycled crustal material in the kimberlite source region could have caused the decoupling of Nd-Hf systematics observed for the Kaavi-Kuopio kimberlites.

We have employed binary mixing models to define the plausible "polluting" components capable of producing the ~9-unit $\varepsilon Hf_{(i)}$ shift observed in the Kaavi-Kuopio kimberlites. For the kimberlite source end member we have utilized the most primitive isotopic compositions from this study (Pipe 1; εNd = ~+1, $\varepsilon Hf_{(i)}$ = ~+6). These Nd-Hf concentrations of the unpolluted kimberlite source (Nd = 1.3 ppm, Hf = 0.25 ppm) are considered to be similar to those of the primitive mantle and the non-chondritic mantle compositions of Palme and O'Neill (2014) and Jackson and Jellinek (2013), respectively, and hence consistent with kimberlite derivation from a close-to-primordial or early depleted reservoir (see Giuliani et al., 2021 for details). In the models,

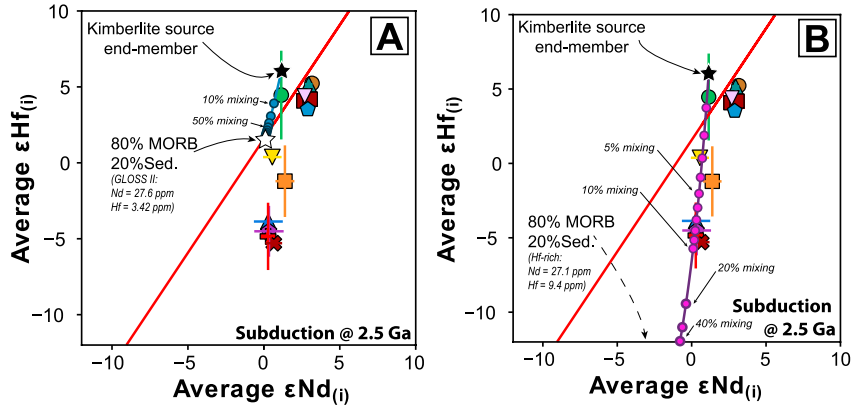

Figure 8. Bivariate plot of $\varepsilon Hf_{(i)}$ versus $\varepsilon Nd_{(i)}$ for the Kaavi-Kuopio kimberlites showing binary mixing relationship between a primitive kimberlite source region with the isotopic composition of Pipe 1 and material subducted at 2.5 Ga. Subducted material is composed of 80% MORB (Gale et al., 2013; Nowell et al., 2004) and 20% Sediment (Sed.) represented by (a) GLOSS II of Plank (2014) and (b) coarse sediment of Bayon et al. (2009). Compositions of subducted component adjusted to account for subduction-induced, sediment-fluid modification following Stracke et al. (2003). See Table S2 in Supporting Information S1 for full model parameters. Symbols as per Figure 5.

this pristine kimberlite source composition was mixed with subducted slab components of varying age and composition, employing the calculations from Stracke et al. (2003) to account for modification of the subducted component(s) (all modeling values supplied in Table. S2 in Supporting Information S1).

These calculations show that the geochemical make-up of altered oceanic crust (i.e., MORB) alone is not sufficiently enriched nor of the correct composition to cause the necessary shifts toward more negative Nd-Hf isotope compositions, regardless of the age of subduction (Figure S6 in Supporting Information S1). Therefore, the sedimentary component of the subducted package must be involved. Our mixing models indicate that the Nd/Hf ratio of this subducted sedimentary component, which represents up to 30% of the recycled material with the remaining being ancient MORB (see below), needs to be lower than the estimate for average modern global subducting sediment (e.g., GLOSS II: Nd = 27.6 ppm, Hf = 3.4 ppm; Plank, 2014, Figure 8a; Figure S7 in Supporting Information S1). It is not implausible for deeply subducted sediment packages to be enriched in Hf; several studies have observed excesses in Hf (and more negative εHf isotopic compositions) in coarse, sand-rich deep ocean trench sediments relative to the finer, clay-rich fractions, a phenomenon generally attributed to zircon accumulation (e.g., Bayon et al., 2009; Carpentier et al., 2009, 2014; Patchett et al., 1984). If Hf contents are elevated as a result of zircon accumulation in the subducted sediments, then correlations between zircon compatible elements and Hf-isotope compositions may be expected. That is, it might be anticipated that a higher "recycled sedimentary" signature in the resulting kimberlite would be expressed by higher Hf and Zr contents and more unradiogenic Hf isotope compositions. Indeed, despite the sedimentary component contributing only a small fraction of the total mass of recycled material, moderate correlations between $\varepsilon Hf_{(i)}$ and whole-rock Hf/Nb and Zr/Nb ratios (Figure 9) are observed and suggest that the unradiogenic-Hf component in the source of the Kaavi-Kuopio kimberlites was enriched in Hf and Zr.

The best fit is obtained by mixing increasing proportions of a subducted package containing 80% N-MORB and 20% Hf-rich sediments (see Figure S8 in Supporting Information S1 for a 90%–10% mixture). The proportion of this material required (5%–30%) varies according to the age of subduction (2–3.5 Ga; Figure 8b; Figures S8, S9 in Supporting Information S1). The timing for the onset of subduction on Earth is not definitively constrained, with estimates ranging from the Hadean to Neo-Archean (e.g., Korenaga, 2013; Korenaga, 2021; Shirey & Richardson, 2011). Therefore, a conservative value of 2.5 Ga for the age of subduction is considered in this model. Our calculations show that the addition of up to ~10% of a 2.5 Ga subducted component consisting of 80% N-MORB + 20% Hf-rich sediments to the kimberlite source region can reproduce the trend in Nd-Hf isotope observed in the Kaavi-Kuopio kimberlites (Figure 8b). Assuming these "polluting" components do not mix and homogenize with the ambient mantle (i.e., they remain as physical entities mingled with ambient mantle material) the correlation between $\varepsilon Hf_{(i)}$ and kimberlite emplacement age (Figure 6) also requires that any entrainment/sampling of this perturbing component must intensify with time and potentially also lower the fO_2

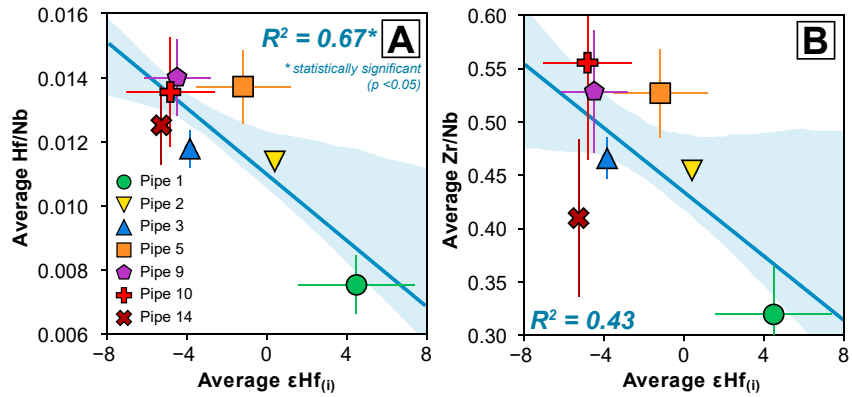

Figure 9. Relationship between average $\varepsilon Hf_{(i)}$ and average whole-rock compositions with regression models fitted for the Kaavi-Kuopio kimberlites. (a) Average Hf/Nb versus average $\varepsilon Hf_{(i)}$; (b) Average Zr/Nb versus average $\varepsilon Hf_{(i)}$. Whole-rock composition data from Dalton, Giuliani, O'Brien, et al. (2020). R^2 is the correlation coefficient, shaded field represents a 1 standard deviation uncertainty envelope. Statistical significance determined using linear regression analysis in the Minitab 20 software package.

of the kimberlite source (Figure 7). Indeed, numerical geodynamic models suggest that streaks or "blobs" of geochemically enriched material can persist in the mantle for timescales up to the age of the Earth (e.g., Ballmer et al., 2017; Gülcher et al., 2020; Jones et al., 2021).

With respective to the relative reduction in fO_2 with decreasing time, it is uncertain whether or not the perovskite and monticellite oxybarometers reflect modification of the source fO_2, as has been suggested for other magma types (Stolper et al., 2020 and references therein), or indicate syn-emplacement degassing or assimilation processes. If degassing is assumed to be an equilibrium process it is unlikely to affect the redox state of the melt relative to a buffer for example, NNO. If these values do indeed reflect source features, then it follows that the link between enriched, less radiogenic isotopic compositions (more negative $\varepsilon Hf_{(i)}$) and more reduced kimberlite melts (more negative ΔNNO) is indicative of a contaminating subducted component that is reduced. It is likely that the deep oceans were reducing until at least 800 Ma (e.g., Lyons et al., 2014; Reinhard & Planavsky, 2020; Stolper & Keller, 2018) and, hence, ancient deep (subducted) sediments were reduced as well. While we acknowledge that the redox state, and mixing mechanisms of ancient, deeply subducted material remain imperfectly understood, the data presented here suggests that progressive incorporation of these sediments into the kimberlite source region not only caused geochemical enrichment (as indicated by decreasing $\varepsilon Hf_{(i)}$ values) but may have also caused the relative reduction in fO_2.

5.3.4. Mantle Plume-Driven Geochemical Enrichment of the Kaavi-Kuopio Kimberlite Source Region

Given our present understanding of the prevailing geodynamic settings at this time (e.g., Murphy et al., 2021; Robert et al., 2021; Tegner et al., 2019), we must first evaluate the possibility of Baltica traversing across a geochemically zoned plume/mantle upwelling or heterogeneous upper mantle before exploring the mechanisms which may permit progressive contamination of the kimberlite source. Such a model is difficult to definitively test given the uncertainties associated with Proterozoic tectonic reconstructions yet it is possible that Baltica drifted several hundred kilometres between 620 Ma and 580 Ma (e.g., Robert et al., 2021). It has been suggested in numerous studies of OIBs (i.e., modern hotspot systems) that geochemical heterogeneities in mantle plumes can give rise to significant geographic compositional zonation in the resultant basaltic magmas (e.g., Abouchami et al., 2005; Hoernle et al., 2015). Further, enhanced plate motion and associated shifts in lithospheric stress regimes have previously been proposed as important triggers for kimberlite emplacement in South Africa and Canada (e.g., Jelsma et al., 2004; Jelsma et al., 2009; Tappe, Brand, et al., 2017). For these mechanisms to hold true in the present case, the Baltic shield would be required to migrate in such a way that it passed over source regions that were systematically becoming isotopically enriched in order to reconcile with the observed temporal trend in isotopic composition of these kimberlites. Such a gradation is unlikely in nature, and in addition, a linear age progression, or any spatiotemporal pattern, such as that observed in several ocean island chains (e.g., Chauvel et al., 2012; Koppers et al., 2011; Williamson et al., 2019) or in the ~250–140 Ma kimberlites and related rocks of the North American Great Meteor hotspot track (Heaman & Kjarsgaard, 2000) is not observed in Finland

despite the protracted time interval of kimberlite eruption. Therefore, while we cannot wholly rule out a model of lithospheric movement over a fixed but geochemically zoned mantle plume/upwelling or a heterogenous upper mantle source region, it is difficult to provide robust evidence in support of such a hypothesis.

Therefore, with plate migration a seemingly unlikely driver, we must now examine the mechanisms by which a recycled component can be increasingly incorporated into the source of the Kaavi-Kuopio kimberlites. In fact, the progressive enrichment in $\varepsilon Hf_{(i)}$ compositions recorded in these kimberlites ($R^2 = 0.72$, $p = 0.02$; Figure 6) is contrary to the expectation that progressive melt extraction from a particular source region would be accompanied by its progressive depletion in geochemically enriched fusible components as observed in the Lac de Gras kimberlite field (Tovey et al., 2021) and hypothesized for basalts globally (e.g., Stracke, 2021; Stracke & Bourdon, 2009).

It was noted earlier (Section 5.3; Figure 4) that the emplacement of the Kaavi-Kuopio kimberlites may be linked to mantle plumes sourced from an LLSVP. A spatiotemporal relationship between LLSVPs and kimberlites was well documented for kimberlites <320 Ma by Torsvik et al. (2010). Giuliani et al. (2021) noted that the PREMA component found in most kimberlite sources may be contained within LLSVPs. However, the distribution of PREMA in the mantle remains uncertain; for example, "blobs/streaks" of ancient material are also modeled to exist and persist throughout the ambient mantle (Ballmer et al., 2017; Becker et al., 1999; Brandenburg et al., 2008; Gülcher et al., 2021; Jones et al., 2021).

An important consideration for an LLSVP-centric geodynamic scenario is that it remains contentious as to whether LLSVPs remain approximately fixed at the core mantle boundary or get swept around/displaced by subducted material (e.g., Ballmer et al., 2017; Bono et al., 2019; Cao et al., 2020; Flament et al., 2017; Niu, 2018; Wolf & Evans, 2021; Young et al., 2019). In the following we assume that these thermochemical piles can persist at the core-mantle boundary on billion-year timescales (e.g., Jones et al., 2021; Yan et al., 2020); however, the outcome of the following model would not change if the source of the Kaavi-Kuopio kimberlites was located in other deep Earth structures where plumes are generated. Despite the contention around LLSVP longevity and fixity, there is agreement for the role of mantle plumes, which emanated from the margins of LLSVPs or other lower mantle sources, in the emplacement of the contemporaneous CIMP and opening the Iapetus ocean (e.g., Ernst & Bell, 2010; Murphy et al., 2021; Robert et al., 2021; Tegner et al., 2019). We also advocate here for a role of these upwellings in the petrogenesis and geochemical evolution of the Kaavi-Kuopio kimberlites (Figure 4; Figure 10).

It is now well-established that mantle plumes are capable of entraining recycled material from deep within the mantle and that this entrained material can alter the geochemistry of the resultant lavas (e.g., Hart et al., 1992; Jackson et al., 2017; Li et al., 2014; Lin and van Keken, 2006; Williams et al., 2015). To replicate the observed pattern in the Kaavi-Kuopio kimberlites, that is, a progressive enrichment of the mantle source with time, we envisage a process whereby a mantle upwelling that taps a primitive kimberlite source reservoir (e.g., PREMA component of Giuliani et al., 2021), progressively incorporates more recycled material (e.g., Figure 10b) across the ~35 Myr period in which the kimberlites were emplaced. In this scenario the lower mantle source region had entrained little to no recycled material (~1%) at the time of Pipe 1 emplacement (~620 Ma; $\varepsilon Hf_{(i)} \sim +4.5$), whereas the upwelling had progressively conveyed increasing proportions (up to 10%) of ancient, subducted crust by the time Pipe 14 was emplaced (~585 Ma; $\varepsilon Hf_{(i)} \sim -5.3$). We focus on entrainment from the lower mantle here as it has been suggested that the geochemistry of plume-derived lavas represents that of their deep-mantle source rather than any significant contributions of material entrained from mid-to upper-mantle depths (e.g., Farnetani & Richards, 1995), though we cannot entirely rule out the role of such material (e.g., Sobolev et al., 2016). Indeed, it also remains plausible that upper mantle convective cells, rather than lower-mantle plumes, could be responsible for the transport of subducted material into the kimberlite source region.

However, this progressive entrainment mechanism is entirely consistent with numerical models and simulations that depict plumes "dragging" compositionally dense materials upwards from the lower mantle (e.g., Li, 2021; Li et al., 2014; Sleep, 1988). While our understanding of material transfer from the lower mantle remains incomplete, the flux of subducted material suggested here, from 1% to 10%, is consistent with numerical modeling (e.g., Tackley, 1998) and laboratory experiments (e.g., Davaille et al., 2002; Jellinek & Manga, 2002; Kumagai et al., 2008) utilized to estimate rates of entrainment in mantle plumes. Absolute rates are dependent on the intrinsic thermal and buoyancy properties of the plume and can range from 0.1% to 15% by volume relative to

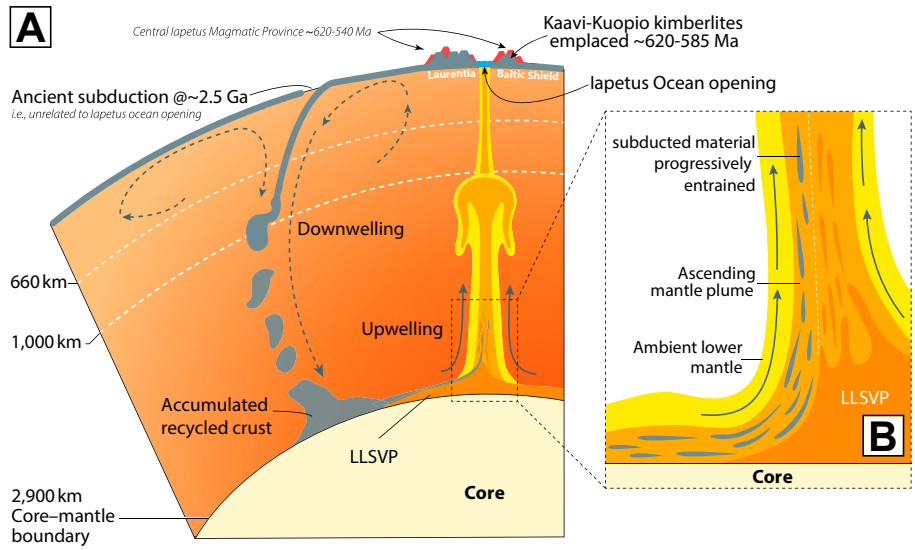

Figure 10. (a) Schematic illustration, modified from Koppers et al. (2021), showing a mantle plume sourced from the margin of an Large Low Shear-wave Velocity Province in the lower mantle. One, or multiple mantle plumes like that shown, are suggested to be involved with the emplacement Central Iapetus Magmatic Province, including the Kaavi-Kuopio kimberlites, and the opening of the Iapetus Ocean between Laurentia and Baltica; (b) close-up view of plume root showing progressive entrainment of subducted material which is considered to modify the composition of the Kaavi-Kuopio kimberlites through progressive enrichment.

total plume flux (Tackley, 2015). In addition, thermo-chemical numerical modeling by Deschamps et al. (2011) suggests that plumes can readily carry up to ~9% of dense recycled material, or in extreme cases, even up to ~21%. These values are consistent with a contribution of up to ~10% of recycled crustal components in the source of the Kaavi-Kuopio kimberlites (Figure 10).

6. Conclusions

The three prominent occurrences of kimberlite and related magmatism in Finland have distinct radiogenic isotopic signatures, indicative of distinctive source regions within the mantle, and like many kimberlite fields throughout the geological record, appear to be inextricably linked to the supercontinent cycle.

The extensional regime associated with the breakup of Laurentia and Baltica at ~1.2 Ga promoted the emplacement of UMLs and olivine lamproites on the Karelian craton. Close-to-chondritic Nd-Hf isotope compositions suggest that the UMLs are predominantly sub-lithospheric melts with minor contribution from metasomatized SCLM material whereas the highly unradiogenic Nd-Hf isotopic composition of olivine lamproites reflect a dominant SCLM component.

In contrast, the timings of kimberlite eruptions at both Kuusamo (~750 Ma) and Kaavi-Kuopio (~600 Ma) appear to bookend the beginning and end of Rodinia break up and the opening of the Iapetus ocean, both probably triggered by the impingement of one or more mantle plumes. The stark contrast in isotopic compositions of these two occurrences, separated by ~300 km and ~150 Myr, is remarkable. The Kuusamo kimberlites have Sr-Nd-Hf compositions that lie precisely on the PREMA trend for kimberlites globally and their near-invariant compositions are indicative of a source that was seemingly homogenous across the ~10 Myr period in which magmatism occurred. In contrast, the Kaavi-Kuopio kimberlites are distinct and become increasingly enriched, with more negative radiogenic isotope compositions (i.e., more negative $\varepsilon Hf_{(i)}$) from ~620 to ~585 Ma. Geochemical modeling and thermodynamic calculations show that this temporal trend cannot be readily explained by lithospheric mantle assimilation, variable melting temperature or lithospheric thickness (and hence pressure of melting assuming melt extraction at the LAB). We propose instead that temporal variations in the Kaavi-Kuopio kimberlites are due to a PREMA-like source region that became progressively enriched with up to 10% of deeply subducted material. In this scenario it is anticipated that progressively more recycled material is entrained by the lower mantle plume source which imparts this time-dependent geochemically enriched signal. These findings are

consistent with ongoing research related to our understanding of mantle plume dynamics and provide additional constraints on how the flux of plume-entrained material from the lower mantle might change with time.

Data Availability Statement

Data for this manuscript can be accessed at The University of Melbourne figshare repository: https://doi.org/10.26188/626ba3ee4e1a3.

Acknowledgments
This work was supported by an Australian Research Training Program PhD Scholarship, Society of Economic Geology Student Research Grant (SRG 18–43) and Geological Society of Australia – Victoria Division student award to HD, and a Swiss National Science Foundation (SNSF) Ambizione fellowship (n. PZ00P2_180126/1) to AG. We would like to thank the Geological Survey of Finland (GTK) for providing access to their drill-core storage facility and making this project possible. We are grateful to Marja Lehtonen and Petri Peltonen for providing access to their xenocryst and xenolith data. HD thanks Graham Hutchinson for his analytical help during SEM sessions, Matthew Felgate and Abaz Alimanovic for mineral separation guidance and Ashlea Wainwright and Serene Paul for assistance with column chemistry procedures. Michael Anenburg and Noah Planavsky are thanked for discussions on fO_2 and HD thanks Zachary Sudholz for assistance with FITPLOT. Trond Torsvik and Nicolas Flament are thanked for support with tectonic reconstructions. Finally, we would like to thank three anonymous reviewers for their detailed feedback which improved this manuscript and Janne Blichert-Toft for her consideration and editorial handling.

References

Abouchami, W., Hofmann, A. W., Galer, S. J. G., Frey, F. A., Eisele, J., & Feigenson, M. (2005). Lead isotopes reveal bilateral asymmetry and vertical continuity in the Hawaiian mantle plume. *Nature*, *434*(7035), 851–856. https://doi.org/10.1038/nature03402

Bailey, D. G., & Lupulescu, M. V. (2015). Spatial, temporal, mineralogical, and compositional variations in Mesozoic kimberlitic magmatism in New York State. *Lithos*, *212*, 298–310. https://doi.org/10.1016/j.lithos.2014.11.022

Ballhaus, C., Berry, R. F., & Green, D. H. (1994). High-pressure experimental calibration of the olivine-orthopyroxene-spinel oxygen geobarometer: Implications for the oxidation state of the upper mantle. *Contributions to Mineralogy and Petrology*, *118*(1), 109–140. https://doi.org/10.1007/bf00311183

Ballmer, M. D., Houser, C., Hernlund, J. W., Wentzcovitch, R. M., & Hirose, K. (2017). Persistence of strong silica-enriched domains in the Earth's lower mantle. *Nature Geoscience*, *10*(3), 236–240. https://doi.org/10.1038/ngeo2898

Bayon, G., Burton, K., Soulet, G., Vigier, N., Dennielou, B., Etoubleau, J., et al. (2009). Hf and Nd isotopes in marine sediments: Constraints on global silicate weathering. *Earth and Planetary Science Letters*, *277*(3), 318–326. https://doi.org/10.1016/j.epsl.2008.10.028

Becker, M., & le Roex, A. P. (2006). Geochemistry of South African on- and off-craton, Group I and Group II kimberlites: Petrogenesis and source region evolution. *Journal of Petrology*, *47*(4), 673–703. https://doi.org/10.1093/petrology/egi089

Becker, T. W., Kellogg, J. B., & O'Connell, R. J. (1999). Thermal constraints on the survival of primitive blobs in the lower mantle. *Earth and Planetary Science Letters*, *171*(3), 351–365. https://doi.org/10.1016/s0012-821x(99)00160-0

Bellis, A., & Canil, D. (2007). Ferric iron in $CaTiO_3$ perovskite as an oxygen barometer for kimberlitic magmas I: Experimental calibration. *Journal of Petrology*, *48*(2), 219–230. https://doi.org/10.1093/petrology/egl054

Bingen, B., Demaiffe, D., & Breemen, O. V. (1998). The 616 Ma old Egersund basaltic dike swarm, sw Norway, and late neoproterozoic opening of the Iapetus ocean. *The Journal of Geology*, *106*(5), 565–574. https://doi.org/10.1086/516042

Bingen, B., Mansfeld, J., Sigmond, E. M. O., & Stein, H. (2002). Baltica-laurentia link during the mesoproterozoic: 1.27 Ga development of continental basins in the sveconorwegian orogen, southern Norway. *Canadian Journal of Earth Sciences*, *39*(9), 1425–1440. https://doi.org/10.1139/e02-054

Bogdanova, S. V., Bingen, B., Gorbatschev, R., Kheraskova, T., Kozlov, V., Puchkov, V., & Volozh, Y. (2008). The East European craton (Baltica) before and during the assembly of Rodinia. *Precambrian Research*, *160*(1–2), 23–45. https://doi.org/10.1016/j.precamres.2007.04.024

Bono, R. K., Tarduno, J. A., & Bunge, H.-P. (2019). Hotspot motion caused the Hawaiian-Emperor Bend and LLSVPs are not fixed. *Nature Communications*, *10*(1), 3370. https://doi.org/10.1038/s41467-019-11314-6

Bouvier, A., Vervoort, J. D., & Patchett, P. J. (2008). The Lu–Hf and Sm–Nd isotopic composition of CHUR: Constraints from unequilibrated chondrites and implications for the bulk composition of terrestrial planets. *Earth and Planetary Science Letters*, *273*(1), 48–57. https://doi.org/10.1016/j.epsl.2008.06.010

Brandenburg, J. P., Hauri, E. H., van Keken, P. E., & Ballentine, C. J. (2008). A multiple-system study of the geochemical evolution of the mantle with force-balanced plates and thermochemical effects. *Earth and Planetary Science Letters*, *276*(1), 1–13. https://doi.org/10.1016/j.epsl.2008.08.027

Burke, K. (2011). Plate tectonics, the Wilson cycle, and mantle plumes: Geodynamics from the top. *Annual Review of Earth and Planetary Sciences*, *39*(1), 1–29. https://doi.org/10.1146/annurev-earth-040809-152521

Canil, D., & Bellis, A. J. (2007). Ferric iron in $CaTiO_3$ perovskite as an oxygen barometer for kimberlite magmas II: Applications. *Journal of Petrology*, *48*(2), 231–252. https://doi.org/10.1093/petrology/egl067

Cao, X., Flament, N., & Müller, R. D. (2020). Coupled evolution of plate tectonics and basal mantle structure. *Geochemistry, Geophysics, Geosystems*, *21*(1), e2020GC009244. https://doi.org/10.1029/2020gc009244

Carpentier, M., Chauvel, C., Maury, R. C., & Mattielli, N. (2009). The "zircon effect" as recorded by the chemical and Hf isotopic compositions of Lesser Antilles forearc sediments. *Earth and Planetary Science Letters*, *287*(1), 86–99. https://doi.org/10.1016/j.epsl.2009.07.043

Carpentier, M., Weis, D., & Chauvel, C. (2014). Fractionation of Sr and Hf isotopes by mineral sorting in Cascadia Basin terrigenous sediments. *Chemical Geology*, *382*, 67–82. https://doi.org/10.1016/j.chemgeo.2014.05.028

Cawood, P. A., McCausland, P. J., & Dunning, G. R. (2001). Opening Iapetus: Constraints from the laurentian margin in newfoundland. *The Geological Society of America Bulletin*, *113*(4), 443–453. https://doi.org/10.1130/0016-7606(2001)113<0443:oicftl>2.0.co;2

Cawood, P. A., & Pisarevsky, S. A. (2006). Was Baltica right-way-up or upside-down in the neoproterozoic? *Journal of the Geological Society*, *163*(5), 753–759. https://doi.org/10.1144/0016-76492005-126

Chalapathi Rao, N. V., Lehmann, B., Belyatsky, B., & Warnsloh, J. M. (2017). The Late Cretaceous diamondiferous pyroclastic kimberlites from the Fort à la Corne (FALC) field, Saskatchewan craton, Canada: Petrology, geochemistry and Genesis. *Gondwana Research*, *44*, 236–257. https://doi.org/10.1016/j.gr.2016.12.013

Chauvel, C., Maury, R. C., Blais, S., Lewin, E., Guillou, H., Guille, G., et al. (2012). The size of plume heterogeneities constrained by Marquesas isotopic stripes. *Geochemistry, Geophysics, Geosystems*, *13*(7). https://doi.org/10.1029/2012gc004123

Choukroun, M., O'Reilly, S. Y., Griffin, W. L., Pearson, N. J., & Dawson, J. B. (2005). Hf isotopes of MARID (mica-amphibole-rutile-ilmenite-diopside) rutile trace metasomatic processes in the lithospheric mantle. *Geology*, *33*(1), 45–48. https://doi.org/10.1130/g21084.1

Coe, N., le Roex, A., Gurney, J., Pearson, D. G., & Nowell, G. (2008). Petrogenesis of the swartruggens and star Group II kimberlite dyke swarms, South Africa: Constraints from whole rock geochemistry. *Contributions to Mineralogy and Petrology*, *156*(5), 627–652. https://doi.org/10.1007/s00410-008-0305-1

Currie, C. A., & Beaumont, C. (2011). Are diamond-bearing Cretaceous kimberlites related to low-angle subduction beneath Western North America? *Earth and Planetary Science Letters*, *303*(1), 59–70. https://doi.org/10.1016/j.epsl.2010.12.036

Dalton, H., Giuliani, A., O'Brien, H., Phillips, D., & Hergt, J. (2020). The role of lithospheric heterogeneity on the composition of kimberlite magmas from a single field: The case of Kaavi-Kuopio, Finland. *Lithos*, *354–355*, 105333. https://doi.org/10.1016/j.lithos.2019.105333

Dalton, H., Giuliani, A., Phillips, D., Hergt, J., Maas, R., Matchan, E., et al. (2020). A comparison of geochronological methods commonly applied to kimberlites and related rocks: Three case studies from Finland. *Chemical Geology*, *558*, 119899. https://doi.org/10.1016/j.chemgeo.2020.119899

Dalton, H. B., Giuliani, A., O'Brien, H., Phillips, D., Hergt, J., & Maas, R. (2019). Petrogenesis of a hybrid cluster of evolved kimberlites and ultramafic lamprophyres in the Kuusamo area, Finland. *Journal of Petrology*, *60*(10), 2025–2050. https://doi.org/10.1093/petrology/egz062

Davaille, A., Girard, F., & Le Bars, M. (2002). How to anchor hotspots in a convecting mantle? *Earth and Planetary Science Letters*, *203*(2), 621–634. https://doi.org/10.1016/s0012-821x(02)00897-x

Dawson, J., Hill, P., & Kinny, P. (2001). Mineral chemistry of a zircon-bearing, composite, veined and metasomatised upper-mantle peridotite xenolith from kimberlite. *Contributions to Mineralogy and Petrology*, *140*(6), 720–733. https://doi.org/10.1007/s004100000216

Deschamps, F., Kaminski, E., & Tackley, P. J. (2011). A deep mantle origin for the primitive signature of ocean island basalt. *Nature Geoscience*, *4*(12), 879–882. https://doi.org/10.1038/ngeo1295

Doig, R. (1970). An alkaline rock province linking Europe and North America. *Canadian Journal of Earth Sciences*, *7*(1), 22–28. https://doi.org/10.1139/e70-002

Duke, G. I., Carlson, R. W., Frost, C. D., Hearn, B. C., Jr., & Eby, G. N. (2014). Continent-scale linearity of kimberlite–carbonatite magmatism, mid-continent North America. *Earth and Planetary Science Letters*, *403*, 1–14. https://doi.org/10.1016/j.epsl.2014.06.023

Ernst, R. E. (2014). *Large igneous provinces*. Cambridge University Press.

Ernst, R. E., & Bell, K. (2010). Large igneous provinces (LIPs) and carbonatites. *Mineralogy and Petrology*, *98*(1), 55–76. https://doi.org/10.1007/s00710-009-0074-1

Ernst, R. E., Liikane, D. A., Jowitt, S. M., Buchan, K. L., & Blanchard, J. A. (2019). A new plumbing system framework for mantle plume-related continental Large Igneous Provinces and their mafic-ultramafic intrusions. *Journal of Volcanology and Geothermal Research*, *384*, 75–84. https://doi.org/10.1016/j.jvolgeores.2019.07.007

Farnetani, D. G., & Richards, M. A. (1995). Thermal entrainment and melting in mantle plumes. *Earth and Planetary Science Letters*, *136*(3), 251–267. https://doi.org/10.1016/0012-821x(95)00158-9

Fedortchouk, Y., & Canil, D. (2004). Intensive variables in kimberlite magmas, lac de Gras, Canada and implications for diamond survival. *Journal of Petrology*, *45*(9), 1725–1745. https://doi.org/10.1093/petrology/egh031

Fitzpayne, A., Giuliani, A., Hergt, J., Phillips, D., & Janney, P. (2018). New geochemical constraints on the origins of MARID and PIC rocks: Implications for mantle metasomatism and mantle-derived potassic magmatism. *Lithos*, *318–319*, 478–493. https://doi.org/10.1016/j.lithos.2018.08.036

Fitzpayne, A., Giuliani, A., Hergt, J., Woodhead, J. D., & Maas, R. (2020). Isotopic analyses of clinopyroxenes demonstrate the effects of kimberlite melt metasomatism upon the lithospheric mantle. *Lithos*, *370–371*, 105595. https://doi.org/10.1016/j.lithos.2020.105595

Fitzpayne, A., Giuliani, A., Maas, R., Hergt, J., Janney, P., & Phillips, D. (2019). Progressive metasomatism of the mantle by kimberlite melts: Sr–Nd–Hf–Pb isotope compositions of MARID and PIC minerals. *Earth and Planetary Science Letters*, *509*, 15–26. https://doi.org/10.1016/j.epsl.2018.12.013

Fitzpayne, A., Giuliani, A., Magalhaes, N., Soltys, A., Fiorentini, M. L., & Farquhar, J. (2021). Sulfur isotope constraints on the petrogenesis of the Kimberley kimberlites. *Geochemistry, Geophysics, Geosystems*, *22*(11), e2021GC009845. https://doi.org/10.1029/2021gc009845

Flament, N., Williams, S., Müller, R. D., Gurnis, M., & Bower, D. J. (2017). Origin and evolution of the deep thermochemical structure beneath Eurasia. *Nature Communications*, *8*(1), 14164. https://doi.org/10.1038/ncomms14164

Foley, S. F., & Fischer, T. P. (2017). An essential role for continental rifts and lithosphere in the deep carbon cycle. *Nature Geoscience*, *10*(12), 897–902. https://doi.org/10.1038/s41561-017-0002-7

Foley, S. F., Yaxley, G. M., & Kjarsgaard, B. A. (2019). Kimberlites from source to surface: Insights from experiments. *Elements*, *15*(6), 393–398. https://doi.org/10.2138/gselements.15.6.393

Fraser, K. J., Hawkesworth, C. J., Erlank, A. J., Mitchell, R. H., & Scott-Smith, B. H. (1985). Sr, Nd and Pb isotope and minor element geochemistry of lamproites and kimberlites. *Earth and Planetary Science Letters*, *76*(1), 57–70. https://doi.org/10.1016/0012-821x(85)90148-7

Gale, A., Dalton, C. A., Langmuir, C. H., Su, Y., & Schilling, J.-G. (2013). The mean composition of ocean ridge basalts. *Geochemistry, Geophysics, Geosystems*, *14*(3), 489–518. https://doi.org/10.1029/2012gc004334

Giuliani, A., Drysdale, R. N., Woodhead, J. D., Planavsky, N. J., Phillips, D., Hergt, J., et al. (2022). Perturbation of the deep-Earth carbon cycle in response to the Cambrian Explosion. *Science Advances*, *8*(9), eabj1325. https://doi.org/10.1126/sciadv.abj1325

Giuliani, A., Jackson, M. G., Fitzpayne, A., & Dalton, H. (2021). Remnants of early Earth differentiation in the deepest mantle-derived lavas. *Proceedings of the National Academy of Sciences*, *118*(1), e2015211118. https://doi.org/10.1073/pnas.2015211118

Giuliani, A., Kamenetsky, V., Kendrick, M., Phillips, D., Wyatt, B., & Maas, R. (2013). Oxide, sulphide and carbonate minerals in a mantle polymict breccia: Metasomatism by proto-kimberlite magmas, and relationship to the kimberlite megacrystic suite. *Chemical Geology*, *353*, 4–18. https://doi.org/10.1016/j.chemgeo.2012.09.025

Giuliani, A., & Pearson, D. G. (2019). Kimberlites: From deep Earth to diamond mines. *Elements*, *15*(6), 377–380. https://doi.org/10.2138/gselements.15.6.377

Giuliani, A., Pearson, D. G., Soltys, A., Dalton, H., Phillips, D., Foley, S. F., et al. (2020a). Kimberlite Genesis from a common carbonate-rich primary melt modified by lithospheric mantle assimilation. *Science Advances*, *6*(17), eaaz0424. https://doi.org/10.1126/sciadv.aaz0424

Giuliani, A., Pearson, D. G., Soltys, A., Dalton, H., Phillips, D., Foley, S. F., et al. (2020b). Kimberlite Genesis from a common carbonate-rich primary melt modified by lithospheric mantle assimilation. *Science Advances*, *6*(14). https://doi.org/10.1126/sciadv.aaz0424

Giuliani, A., Phillips, D., Kamenetsky, V. S., Fiorentini, M. L., Farquhar, J., & Kendrick, M. A. (2014). Stable isotope (C, O, S) compositions of volatile-rich minerals in kimberlites: A review. *Chemical Geology*, *374–375*, 61–83. https://doi.org/10.1016/j.chemgeo.2014.03.003

Giuliani, A., Phillips, D., Kamenetsky, V. S., & Goemann, K. (2016). Constraints on kimberlite ascent mechanisms revealed by phlogopite compositions in kimberlites and mantle xenoliths. *Lithos*, *240–243*, 189–201. https://doi.org/10.1016/j.lithos.2015.11.013

Giuliani, A., Phillips, D., Woodhead, J. D., Kamenetsky, V. S., Fiorentini, M. L., Maas, R., et al. (2015). Did diamond-bearing orangeites originate from MARID-veined peridotites in the lithospheric mantle? *Nature Communications*, *6*(1), 6837. https://doi.org/10.1038/ncomms7837

Grant, T. B., Larsen, R. B., Brown, E. L., Müller, A. B., & McEnroe, S. (2020). Mixing of heterogeneous, high-MgO, plume-derived magmas at the base of the crust in the Central Iapetus Magmatic Province (Ma 610-550): Origin of parental magmas to a global LIP event. *Lithos*, *364–365*, 105535. https://doi.org/10.1016/j.lithos.2020.105535

Grégoire, M., Bell, D., & Le Roex, A. (2002). Trace element geochemistry of phlogopite-rich mafic mantle xenoliths: Their classification and their relationship to phlogopite-bearing peridotites and kimberlites revisited. *Contributions to Mineralogy and Petrology*, *142*(5), 603–625. https://doi.org/10.1007/s00410-001-0315-8

Gudfinnsson, G. H., & Presnall, D. C. (2005). Continuous gradations among primary carbonatitic, kimberlitic, melilititic, basaltic, picritic, and komatiitic melts in equilibrium with garnet lherzolite at 3–8 GPa. *Journal of Petrology*, *46*(8), 1645–1659. https://doi.org/10.1093/petrology/egi029

Gülcher, A. J. P., Ballmer, M. D., & Tackley, P. J. (2021). Coupled dynamics and evolution of primordial and recycled heterogeneity in Earth's lower mantle. *Solid Earth*, *12*(9), 2087–2107. https://doi.org/10.5194/se-12-2087-2021

Gülcher, A. J. P., Gebhardt, D. J., Ballmer, M. D., & Tackley, P. J. (2020). Variable dynamic styles of primordial heterogeneity preservation in the Earth's lower mantle. *Earth and Planetary Science Letters*, *536*, 116160. https://doi.org/10.1016/j.epsl.2020.116160

Hart, S. R., Hauri, E. H., Oschmann, L. A., & Whitehead, J. A. (1992). Mantle plumes and entrainment: Isotopic evidence. *Science*, *256*(5056), 517–520. https://doi.org/10.1126/science.256.5056.517

Harte, B., & Harris, J. (1994). Lower mantle mineral associations preserved in diamonds. *Mineralogical Magazine*, *58*(1), 384–385. https://doi.org/10.1180/minmag.1994.58a.1.201

Hartz, E. H., & Torsvik, T. H. (2002). Baltica upside down: A new plate tectonic model for Rodinia and the Iapetus ocean. *Geology*, *30*(3), 255–258. https://doi.org/10.1130/0091-7613(2002)030<0255:budanp>2.0.co;2

Heaman, L. M., & Kjarsgaard, B. A. (2000). Timing of eastern North American kimberlite magmatism: Continental extension of the great meteor hotspot track? *Earth and Planetary Science Letters*, *178*(3–4), 253–268. https://doi.org/10.1016/s0012-821x(00)00079-0

Heaman, L. M., Kjarsgaard, B. A., & Creaser, R. A. (2004). The temporal evolution of North American kimberlites. *Lithos*, *76*(1–4), 377–397. https://doi.org/10.1016/j.lithos.2004.03.047

Heaman, L. M., Phillips, D., & Pearson, G. (2019). Dating kimberlites: Methods and emplacement patterns through time. *Elements*, *15*(6), 399–404. https://doi.org/10.2138/gselements.15.6.399

Helmstaedt, H., & Gurney, J. (1997). Geodynamic controls of kimberlites-what are the roles of hotspot and plate tectonics? *Russian Geology and Geophysics*, *38*, 492–508.

Hoernle, K., Rohde, J., Hauff, F., Garbe-Schonberg, D., Homrighausen, S., Werner, R., & Morgan, J. P. (2015). How and when plume zonation appeared during the 132 Myr evolution of the Tristan Hotspot. *Nature Communications*, *6*(1), 7799. https://doi.org/10.1038/ncomms8799

Ito, G., & Mahoney, J. J. (2005a). Flow and melting of a heterogeneous mantle: 1. Method and importance to the geochemistry of ocean island and mid-ocean ridge basalts. *Earth and Planetary Science Letters*, *230*(1), 29–46. https://doi.org/10.1016/j.epsl.2004.10.035

Ito, G., & Mahoney, J. J. (2005b). Flow and melting of a heterogeneous mantle: 2. Implications for a chemically nonlayered mantle. *Earth and Planetary Science Letters*, *230*(1), 47–63. https://doi.org/10.1016/j.epsl.2004.10.034

Jackson, M. G., & Jellinek, A. M. (2013). Major and trace element composition of the high 3He/4He mantle: Implications for the composition of a nonchonditic Earth. *Geochemistry, Geophysics, Geosystems*, *14*(8), 2954–2976. https://doi.org/10.1002/ggge.20188

Jackson, M. G., Konter, J. G., & Becker, T. W. (2017). Primordial helium entrained by the hottest mantle plumes. *Nature*, *542*(7641), 340–343. https://doi.org/10.1038/nature21023

Jellinek, A. M., & Manga, M. (2002). The influence of a chemical boundary layer on the fixity, spacing and lifetime of mantle plumes. *Nature*, *418*(6899), 760–763. https://doi.org/10.1038/nature00979

Jelsma, H., Barnett, W., Richards, S., & Lister, G. (2009). Tectonic setting of kimberlites. *Lithos*, *112*, 155–165. https://doi.org/10.1016/j.lithos.2009.06.030

Jelsma, H. A., de Wit, M. J., Thiart, C., Dirks, P. H. G. M., Viola, G., Basson, I., et al. (2004). Preferential distribution along transcontinental corridors of kimberlites and related rocks of Southern Africa. *South African Journal of Geology*, *107*(1/2), 301–324. https://doi.org/10.2113/107.1-2.301

Johansson, Å. (2014). From Rodinia to gondwana with the 'SAMBA' model—A distant view from Baltica towards Amazonia and beyond. *Precambrian Research*, *244*, 226–235. https://doi.org/10.1016/j.precamres.2013.10.012

Jones, T. D., Sime, N., & van Keken, P. E. (2021). Burying Earth's primitive mantle in the slab graveyard. *Geochemistry, Geophysics, Geosystems*, *22*(3), e2020GC009396. https://doi.org/10.1029/2020gc009396

Kamber, B. S., Greig, A., Schoenberg, R., & Collerson, K. D. (2003). A refined solution to Earth's hidden niobium: Implications for evolution of continental crust and mode of core formation. *Precambrian Research*, *126*(3), 289–308. https://doi.org/10.1016/s0301-9268(03)00100-1

Kaminsky, F. (2012). Mineralogy of the lower mantle: A review of 'super-deep' mineral inclusions in diamond. *Earth-Science Reviews*, *110*(1), 127–147. https://doi.org/10.1016/j.earscirev.2011.10.005

Kamo, S. L., Gower, C. F., & Krogh, T. E. (1989). Birthdate for the lapetus ocean? A precise U-Pb zircon and baddeleyite age for the long range dikes, southeast labrador. *Geology*, *17*(7), 602–605. https://doi.org/10.1130/0091-7613(1989)017<0602:bftloa>2.3.co;2

Kargin, A. V., Nosova, A. A., Larionova, Y. O., Kononova, V. A., Borisovsky, S. E., Koval'chuk, E. V., & Griboedova, I. G. (2014). Mesoproterozoic orangeites (kimberlites II) of west karelia: Mineralogy, geochemistry, and Sr-Nd isotope composition. *Petrology*, *22*(2), 151–183. https://doi.org/10.1134/s0869591114020039

Kjarsgaard, B. A., Heaman, L. M., Sarkar, C., & Pearson, D. G. (2017). The North America mid-Cretaceous kimberlite corridor: Wet, edge-driven decompression melting of an OIB-type deep mantle source. *Geochemistry, Geophysics, Geosystems*, *18*(7), 2727–2747. https://doi.org/10.1002/2016gc006761

Konzett, J., Armstrong, R. A., Sweeney, R. J., & Compston, W. (1998). The timing of MARID metasomatism in the Kaapvaal mantle: An ion probe study of zircons from MARID xenoliths. *Earth and Planetary Science Letters*, *160*(1), 133–145. https://doi.org/10.1016/s0012-821x(98)00073-9

Koppers, A. A. P., Gowen, M. D., Colwell, L. E., Gee, J. S., Lonsdale, P. F., Mahoney, J. J., & Duncan, R. A. (2011). New 40Ar/39Ar age progression for the Louisville hot spot trail and implications for inter–hot spot motion. *Geochemistry, Geophysics, Geosystems*, *12*(12). https://doi.org/10.1029/2011gc003804

Korenaga, J. (2013). Initiation and evolution of plate tectonics on Earth: Theories and observations. *Annual Review of Earth and Planetary Sciences*, *41*(1), 117–151. https://doi.org/10.1146/annurev-earth-050212-124208

Korenaga, J. (2021). Hadean geodynamics and the nature of early continental crust. *Precambrian Research*, *359*, 106178. https://doi.org/10.1016/j.precamres.2021.106178

Kumagai, I., Davaille, A., Kurita, K., & Stutzmann, E. (2008). Mantle plumes: Thin, fat, successful, or failing? Constraints to explain hot spot volcanism through time and space. *Geophysical Research Letters*, *35*(16), L16301. https://doi.org/10.1029/2008gl035079

Larsen, L. M., & Rex, D. C. (1992). A review of the 2500 Ma span of alkaline-ultramafic, potassic and carbonatitic magmatism in West Greenland. *Lithos*, *28*(3), 367–402. https://doi.org/10.1016/0024-4937(92)90015-q

Le Pioufle, A., & Canil, D. (2012). Iron in monticellite as an oxygen barometer for kimberlite magmas. *Contributions to Mineralogy and Petrology*, *163*(6), 1033–1046. https://doi.org/10.1007/s00410-011-0714-4

le Roex, A. P., Bell, D. R., & Davis, P. (2003). Petrogenesis of Group I kimberlites from Kimberley, South Africa: Evidence from bulk-rock geochemistry. *Journal of Petrology*, *44*(12), 2261–2286. https://doi.org/10.1093/petrology/egg077

Lehtonen, M., & O'Brien, H. (2009). Mantle transect of the Karelian Craton from margin to core based on PT data from garnet and clinopyroxene xenocrysts in kimberlites. *Bulletin of the Geological Society of Finland*, *81*(2), 79–102. https://doi.org/10.17741/bgsf/81.2.001

Li, M. (2021). The cycling of subducted oceanic crust in the Earth's deep mantle. In H. Marquardt, M. D. Ballmer, S. Cottaar, & J. Konter (Eds.), *Mantle convection and surface expressions* (pp. 303–328). American Geophysical Union.

Li, M., McNamara, A. K., & Garnero, E. J. (2014). Chemical complexity of hotspots caused by cycling oceanic crust through mantle reservoirs. *Nature Geoscience*, *7*(5), 366–370. https://doi.org/10.1038/ngeo2120

Li, Z. X., Bogdanova, S., Collins, A., Davidson, A., De Waele, B., Ernst, R., et al. (2008). Assembly, configuration, and break-up history of Rodinia: A synthesis. *Precambrian Research*, *160*(1–2), 179–210. https://doi.org/10.1016/j.precamres.2007.04.021

Lin, S.-C., & van Keken, P. E. (2006). Dynamics of thermochemical plumes: 1. Plume formation and entrainment of a dense layer. *Geochemistry, Geophysics, Geosystems*, *7*(2). https://doi.org/10.1029/2005gc001071

Lyons, T. W., Reinhard, C. T., & Planavsky, N. J. (2014). The rise of oxygen in Earth's early ocean and atmosphere. *Nature*, *506*(7488), 307–315. https://doi.org/10.1038/nature13068

Massuyeau, M., Gardes, E., Rogerie, G., Aulbach, S., Tappe, S., Le Trong, E., et al. (2021). Maglab: A computing platform connecting geophysical signatures to melting processes in Earth's mantle. *Physics of the Earth and Planetary Interiors*, *314*, 106638. https://doi.org/10.1016/j.pepi.2020.106638

Mather, K. A., Pearson, D. G., McKenzie, D., Kjarsgaard, B. A., & Priestley, K. (2011). Constraints on the depth and thermal history of cratonic lithosphere from peridotite xenoliths, xenocrysts and seismology. *Lithos*, *125*(1), 729–742. https://doi.org/10.1016/j.lithos.2011.04.003

McCandless, T. (1999). Kimberlites: Mantle expressions of deep-seated subduction. *Proceedings of the 7th international kimberlite conference*, 545–549.

Meert, J. G., Walderhaug, H. J., Torsvik, T. H., & Hendriks, B. W. H. (2007). Age and paleomagnetic signature of the Alnø carbonatite complex (NE Sweden): Additional controversy for the Neoproterozoic paleoposition of Baltica. *Precambrian Research*, *154*(3), 159–174. https://doi.org/10.1016/j.precamres.2006.12.008

Merdith, A. S., Collins, A. S., Williams, S. E., Pisarevsky, S., Foden, J. D., Archibald, D. B., et al. (2017). A full-plate global reconstruction of the Neoproterozoic. *Gondwana Research*, *50*, 84–134. https://doi.org/10.1016/j.gr.2017.04.001

Merdith, A. S., Williams, S. E., Collins, A. S., Tetley, M. G., Mulder, J. A., Blades, M. L., et al. (2021). Extending full-plate tectonic models into deep time: Linking the Neoproterozoic and the Phanerozoic. *Earth-Science Reviews*, *214*, 103477. https://doi.org/10.1016/j.earscirev.2020.103477

Mertanen, S., & Pesonen, L. J. (2005). Drift history of the shield. In M. Lehtinen, P. A. Nurmi, & O. T. Rämö (Eds.), *Precambrian Geology of Finland - key to the evolution of the fennoscandian shield. Developments in precambrian Geology* (pp. 645–668). Elsevier.

Mitchell, R. H. (1986). *Kimberlites: Mineralogy, geochemistry, and petrology* (p. 442). Springer Science & Business Media.

Moore, A., Blenkinsop, T., & Cotterill, F. (2008). Controls on post-Gondwana alkaline volcanism in Southern Africa. *Earth and Planetary Science Letters*, *268*(1–2), 151–164. https://doi.org/10.1016/j.epsl.2008.01.007

Münker, C., Weyer, S., Scherer, E., & Mezger, K. (2001). Separation of high field strength elements (Nb, Ta, Zr, Hf) and Lu from rock samples for MC-ICPMS measurements. *Geochemistry, Geophysics, Geosystems*, *2*(12). https://doi.org/10.1029/2001gc000183

Murphy, J. B., Nance, R. D., Cawood, P. A., Collins, W. J., Dan, W., Doucet, L. S., et al. (2021). Pannotia: In defence of its existence and geodynamic significance. *Geological Society, London, Special Publications*, *503*(1), 13–39. https://doi.org/10.1144/sp503-2020-96

Nakanishi, N., Giuliani, A., Carlson, R. W., Horan, M. F., Woodhead, J., Pearson, D. G., & Walker, R. J. (2021). Tungsten-182 evidence for an ancient kimberlite source. *Proceedings of the National Academy of Sciences*, *118*(23), e2020680118. https://doi.org/10.1073/pnas.2020680118

Nelson, D. R. (1989). Isotopic characteristics and petrogenesis of the lamproites and kimberlites of central West Greenland. *Lithos*, *22*(4), 265–274. https://doi.org/10.1016/0024-4937(89)90029-7

Nimis, P., & Taylor, W. R. (2000). Single clinopyroxene thermobarometry for garnet peridotites. Part I. Calibration and testing of a Cr-in-Cpx barometer and an enstatite-in-Cpx thermometer. *Contributions to Mineralogy and Petrology*, *139*(5), 541–554. https://doi.org/10.1007/s004100000156

Nironen, M. (2017). *Guide to the geological map of Finland – bedrock 1:1 000 000* (Vol. 60, pp. 41–76). Geological Survey of Finland Special Paper.

Niu, Y. (2018). Origin of the LLSVPs at the base of the mantle is a consequence of plate tectonics – a petrological and geochemical perspective. *Geoscience Frontiers*, *9*(5), 1265–1278. https://doi.org/10.1016/j.gsf.2018.03.005

Nowell, G. M., Pearson, D. G., Bell, D. R., Carlson, R. W., Smith, C. B., Kempton, P. D., & Noble, S. R. (2004). Hf isotope systematics of kimberlites and their megacrysts: New constraints on their source regions. *Journal of Petrology*, *45*(8), 1583–1612. https://doi.org/10.1093/petrology/egh024

O'Brien, H. (2015). Kimberlite-hosted diamonds in Finland. In W. D. Maier, R. Lahtinen, & H. O'Brien (Eds.), *Mineral deposits of Finland* (pp. 345–375). Elsevier.

O'Brien, H., Phillips, D., & Spencer, R. (2007). Isotopic ages of Lentiira-Kuhmo-Kostomuksha olivine lamproite-Group II kimberlites. *Bulletin of the Geological Society of Finland*, *79*(2), 203–215. https://doi.org/10.17741/bgsf/79.2.004

O'Brien, H. E., Peltonen, P., & Vartiainen, H. (2005). Kimberlites, Carbonatites, and alkaline rocks. In M. Lehtinen, P. A. Nurmi, & O. T. Rämö (Eds.), *Precambrian Geology of Finland - key to the evolution of the fennoscandian shield. Developments in precambrian Geology* (pp. 605–644).

O'Brien, H. E., & Tyni, M. (1999). Mineralogy and geochemistry of kimberlites and related rocks from Finland. In *Proceedings of the 7th international kimberlite conference* (pp. 625–636). Red Roof Design cc Cape.

O'Neill, H. S. C., & Wall, V. (1987). The olivine—Orthopyroxene—Spinel oxygen geobarometer, the nickel precipitation curve, and the oxygen fugacity of the Earth's upper mantle. *Journal of Petrology*, *28*(6), 1169–1191. https://doi.org/10.1093/petrology/28.6.1169

Palme, H., & O'Neill, H. S. C. (2014). Cosmochemical estimates of mantle composition. In H. D. Holland & K. K. Turekian (Eds.), *Treatise on geochemistry* (2nd ed., pp. 1–39). Elsevier.

Pandey, A., & Rao, N. V. C. (2020). Supercontinent transition as a trigger for ~1.1 Gyr diamondiferous kimberlites and related magmatism in India. *Lithos*, *370–371*, 105620. https://doi.org/10.1016/j.lithos.2020.105620

Parrish, J. B., & Lavin, P. M. (1982). Tectonic model for kimberlite emplacement in the Appalachian Plateau of Pennsylvania. *Geology*, *10*(7), 344–347. https://doi.org/10.1130/0091-7613(1982)10<344:tmfkei>2.0.co;2

Patchett, P. J., White, W. M., Feldmann, H., Kielinczuk, S., & Hofmann, A. W. (1984). Hafnium/rare Earth element fractionation in the sedimentary system and crustal recycling into the Earth's mantle. *Earth and Planetary Science Letters*, *69*(2), 365–378. https://doi.org/10.1016/0012-821x(84)90195-x

Paton, C., Hergt, J. M., Phillips, D., Woodhead, J. D., & Shee, S. R. (2007). New insights into the Genesis of Indian kimberlites from the Dharwar Craton via in situ Sr isotope analysis of groundmass perovskite. *Geology*, *35*(11), 1011–1014. https://doi.org/10.1130/g24040a.1

Pearson, D. G., Brenker, F. E., Nestola, F., McNeill, J., Nasdala, L., Hutchison, M. T., et al. (2014). Hydrous mantle transition zone indicated by ringwoodite included within diamond. *Nature*, *507*(7491), 221–224. https://doi.org/10.1038/nature13080

Pearson, D. G., Woodhead, J., & Janney, P. E. (2019). Kimberlites as geochemical probes of Earth's mantle. *Elements*, *15*(6), 387–392. https://doi.org/10.2138/gselements.15.6.387

Peltonen, P., Huhma, H., Tyni, M., & Shimizu, N. (1999). Garnet peridotite xenoliths from kimberlites of Finland: Nature of the continental mantle at an archaean craton–proterozoic mobile belt transition. In *Proceedings of the 7th international kimberlite conference* (pp. 664–676). Red Roof Design cc Cape.

Pin, C., Gannoun, A., & Dupont, A. (2014). Rapid, simultaneous separation of Sr, Pb, and Nd by extraction chromatography prior to isotope ratios determination by TIMS and MC-ICP-MS. *Journal of Analytical Atomic Spectrometry*, *29*(10), 1858–1870. https://doi.org/10.1039/c4ja00169a

Plank, T. (2014). 4.17 - the chemical composition of subducting sediments. In H. D. Holland & K. K. Turekian (Eds.), *Treatise on geochemistry* (2nd ed., pp. 607–629). Elsevier.

Puffer, J. H. (2002). A late Neoproterozoic eastern Laurentian superplume: Location, size, chemical composition, and environmental impact. *American Journal of Science*, *302*(1), 1–27. https://doi.org/10.2475/ajs.302.1.1

Ranger, I. M., Heaman, L. M., Pearson, D. G., Muntener, C., & Zhuk, V. (2018). Punctuated, long-lived emplacement history of the Renard 2 kimberlite, Canada, revealed by new high precision U-Pb groundmass perovskite dating. *Mineralogy and Petrology*, *112*(S2), 639–651. https://doi.org/10.1007/s00710-018-0629-0

Reinhard, C. T., & Planavsky, N. J. (2020). Biogeochemical controls on the redox evolution of Earth's oceans and atmosphere. *Elements*, *16*(3), 191–196. https://doi.org/10.2138/gselements.16.3.191

Robert, B., Domeier, M., & Jakob, J. (2020). Iapetan oceans: An analog of tethys? Geology.

Robert, B., Domeier, M., & Jakob, J. (2021). On the origins of the Iapetus ocean. *Earth-Science Reviews*, *221*, 103791. https://doi.org/10.1016/j.earscirev.2021.103791

Rukhlov, A. S., & Bell, K. (2010). Geochronology of carbonatites from the Canadian and baltic shields, and the Canadian cordillera: Clues to mantle evolution. *Mineralogy and Petrology*, *98*(1), 11–54. https://doi.org/10.1007/s00710-009-0054-5

Russell, J. K., Porritt, L. A., Lavallee, Y., & Dingwell, D. B. (2012). Kimberlite ascent by assimilation-fuelled buoyancy. *Nature*, *481*(7381), 352–356. https://doi.org/10.1038/nature10740

Salminen, J., Pesonen, L. J., Mertanen, S., Vuollo, J., & Airo, M.-L. (2009). Palaeomagnetism of the salla diabase dyke, northeastern Finland, and its implication for the baltica-laurentia entity during the mesoproterozoic. *Geological Society, London, Special Publications*, *323*(1), 199–217. https://doi.org/10.1144/sp323.9

Sarkar, S., Giuliani, A., Ghosh, S., & Phillips, D. (2021). Petrogenesis of coeval lamproites and kimberlites from the Wajrakarur field, Southern India: New insights from olivine compositions. *Lithos*, *406–407*, 106524. https://doi.org/10.1016/j.lithos.2021.106524

Secher, K., Heaman, L., Nielsen, T., Jensen, S., Schjoth, F., & Creaser, R. (2009). Timing of kimberlite, carbonatite, and ultramafic lamprophyre emplacement in the alkaline province located 64°–67°N in southern West Greenland. *Lithos*, *112*, 400–406. https://doi.org/10.1016/j.lithos.2009.04.035

Shaikh, A. M., Patel, S. C., Ravi, S., Behera, D., & Pruseth, K. L. (2017). Mineralogy of the TK1 and TK4 'kimberlites' in the Timmasamudram cluster, Wajrakarur Kimberlite Field, India: Implications for lamproite magmatism in a field of kimberlites and ultramafic lamprophyres. *Chemical Geology*, *455*, 208–230. https://doi.org/10.1016/j.chemgeo.2016.10.030

Shirey, S. B., & Richardson, S. H. (2011). Start of the Wilson cycle at 3 Ga shown by diamonds from subcontinental mantle. *Science*, *333*(6041), 434–436. https://doi.org/10.1126/science.1206275

Sleep, N. H. (1988). Gradual entrainment of a chemical layer at the base of the mantle by overlying convection. *Geophysical Journal International*, *95*(3), 437–447. https://doi.org/10.1111/j.1365-246x.1988.tb06695.x

Smith, C. B. (1983). Pb, Sr and Nd isotopic evidence for sources of southern African Cretaceous kimberlites. *Nature*, *304*(5921), 51–54. https://doi.org/10.1038/304051a0

Sobolev, A. V., Asafov, E. V., Gurenko, A. A., Arndt, N. T., Batanova, V. G., Portnyagin, M. V., et al. (2016). Komatiites reveal a hydrous Archaean deep-mantle reservoir. *Nature*, *531*(7596), 628–632. https://doi.org/10.1038/nature17152

Soltys, A., Giuliani, A., Phillips, D., Kamenetsky, V. S., Maas, R., Woodhead, J., & Rodemann, T. (2016). In-situ assimilation of mantle minerals by kimberlitic magmas — Direct evidence from a garnet wehrlite xenolith entrained in the Bultfontein kimberlite (Kimberley, South Africa). *Lithos*, *256–257*, 182–196. https://doi.org/10.1016/j.lithos.2016.04.011

Stachel, T. (2001). Diamonds from the asthenosphere and the transition zone. *European Journal of Mineralogy*, *13*(5), 883–892. https://doi.org/10.1127/0935-1221/2001/0013/0883

Stern, R. J., Leybourne, M. I., & Tsujimori, T. (2016). Kimberlites and the start of plate tectonics. *Geology*, *44*(10), 799–802. https://doi.org/10.1130/g38024.1

Stolper, D. A., & Keller, C. B. (2018). A record of deep-ocean dissolved O2 from the oxidation state of iron in submarine basalts. *Nature*, *553*(7688), 323–327. https://doi.org/10.1038/nature25009

Stolper, E. M., Shorttle, O., Antoshechkina, P. M., & Asimow, P. D. (2020). The effects of solid-solid phase equilibria on the oxygen fugacity of the upper mantle. *American Mineralogist*, *105*(10), 1445–1471. https://doi.org/10.2138/am-2020-7162

Stracke, A. (2021). A process-oriented approach to mantle geochemistry. *Chemical Geology*, *579*, 120350. https://doi.org/10.1016/j.chemgeo.2021.120350

Stracke, A., Bizimis, M., & Salters, V. J. M. (2003). Recycling oceanic crust: Quantitative constraints. *Geochemistry, Geophysics, Geosystems*, *4*(3). https://doi.org/10.1029/2001gc000223

Stracke, A., & Bourdon, B. (2009). The importance of melt extraction for tracing mantle heterogeneity. *Geochimica et Cosmochimica Acta*, *73*(1), 218–238. https://doi.org/10.1016/j.gca.2008.10.015

Tackley, P. J. (1998). Three-dimensional simulations of mantle convection with a thermo-chemical basal boundary layer: D. In M. Gurnis, M. E. Wysession, E. Knittle, & B. A. Buffett (Eds.), *The core-mantle boundary region* (pp. 231–253). AGU.

Tackley, P. J. (2015). Mantle geochemical geodynamics. In G. Schubert (Ed.), *Treatise on geophysics* (2nd ed., pp. 521–585). Elsevier.

Tainton, K. M., & McKenzie, D. A. N. (1994). The generation of kimberlites, lamproites, and their source rocks. *Journal of Petrology*, *35*(3), 787–817. https://doi.org/10.1093/petrology/35.3.787

Tappe, S., Brand, N. B., Stracke, A., van Acken, D., Liu, C. Z., Strauss, H., et al. (2017a). Plates or plumes in the origin of kimberlites: U/Pb perovskite and Sr-Nd-Hf-Os-C-O isotope constraints from the superior craton (Canada). *Chemical Geology*, *455*, 57–83. https://doi.org/10.1016/j.chemgeo.2016.08.019

Tappe, S., Budde, G., Stracke, A., Wilson, A., & Kleine, T. (2020a). The tungsten-182 record of kimberlites above the African superplume: Exploring links to the core-mantle boundary. *Earth and Planetary Science Letters*, *547*, 116473. https://doi.org/10.1016/j.epsl.2020.116473

Tappe, S., Foley, S. F., Kjarsgaard, B. A., Romer, R. L., Heaman, L. M., Stracke, A., & Jenner, G. A. (2008). Between carbonatite and lamproite—Diamondiferous Torngat ultramafic lamprophyres formed by carbonate-fluxed melting of cratonic MARID-type metasomes. *Geochimica et Cosmochimica Acta*, *72*(13), 3258–3286. https://doi.org/10.1016/j.gca.2008.03.008

Tappe, S., Graham Pearson, D., Kjarsgaard, B. A., Nowell, G., & Dowall, D. (2013). Mantle transition zone input to kimberlite magmatism near a subduction zone: Origin of anomalous Nd–Hf isotope systematics at Lac de Gras, Canada. *Earth and Planetary Science Letters*, *371–372*, 235–251. https://doi.org/10.1016/j.epsl.2013.03.039

Tappe, S., Kjarsgaard, B. A., Kurszlaukis, S., Nowell, G. M., & Phillips, D. (2014). Petrology and Nd–Hf isotope geochemistry of the neoproterozoic amon kimberlite sills, baffin island (Canada): Evidence for deep mantle magmatic activity linked to supercontinent cycles. *Journal of Petrology*, *55*(10), 2003–2042. https://doi.org/10.1093/petrology/egu048

Tappe, S., Pearson, D. G., Nowell, G., Nielsen, T., Milstead, P., & Muehlenbachs, K. (2011). A fresh isotopic look at Greenland kimberlites: Cratonic mantle lithosphere imprint on deep source signal. *Earth and Planetary Science Letters*, *305*(1–2), 235–248. https://doi.org/10.1016/j.epsl.2011.03.005

Tappe, S., Romer, R. L., Stracke, A., Steenfelt, A., Smart, K. A., Muehlenbachs, K., & Torsvik, T. H. (2017). Sources and mobility of carbonate melts beneath cratons, with implications for deep carbon cycling, metasomatism and rift initiation. *Earth and Planetary Science Letters*, *466*, 152–167. https://doi.org/10.1016/j.epsl.2017.03.011

Tappe, S., Smart, K., Torsvik, T., Massuyeau, M., & de Wit, M. (2018). Geodynamics of kimberlites on a cooling Earth: Clues to plate tectonic evolution and deep volatile cycles. *Earth and Planetary Science Letters*, *484*, 1–14. https://doi.org/10.1016/j.epsl.2017.12.013

Tappe, S., Stracke, A., van Acken, D., Strauss, H., & Luguet, A. (2020). Origins of kimberlites and carbonatites during continental collision – Insights beyond decoupled Nd-Hf isotopes. *Earth-Science Reviews*, *208*, 103287. https://doi.org/10.1016/j.earscirev.2020.103287

Tegner, C., Andersen, T. B., Kjoll, H. J., Brown, E. L., Hagen-Peter, G., Corfu, F., et al. (2019). A mantle plume origin for the scandinavian dyke complex: A "piercing point" for 615 Ma plate reconstruction of Baltica? *Geochemistry, Geophysics, Geosystems*, *20*(2), 1075–1094. https://doi.org/10.1029/2018gc007941

Torsvik, T. H. (2019). Earth history: A journey in time and space from base to top. *Tectonophysics*, *760*, 297–313. https://doi.org/10.1016/j.tecto.2018.09.009

Torsvik, T. H., Burke, K., Steinberger, B., Webb, S. J., & Ashwal, L. D. (2010). Diamonds sampled by plumes from the core-mantle boundary. *Nature*, *466*(7304), 352–355. https://doi.org/10.1038/nature09216

Tovey, M., Giuliani, A., Phillips, D., Pearson, D. G., Sarkar, C., Nowicki, T., & Carlson, J. (2021). The spatial and temporal evolution of primitive melt compositions within the Lac de Gras kimberlite field, Canada: Source evolution vs lithospheric mantle assimilation. *Lithos*, *392–393*, 106142. https://doi.org/10.1016/j.lithos.2021.106142

Upton, B. G. J., Emeleus, C. H., Heaman, L. M., Goodenough, K. M., & Finch, A. A. (2003). Magmatism of the mid-proterozoic gardar province, South Greenland: Chronology, petrogenesis and geological setting. *Lithos*, *68*(1), 43–65. https://doi.org/10.1016/s0024-4937(03)00030-6

Vervoort, J. D., Plank, T., & Prytulak, J. (2011). The Hf–Nd isotopic composition of marine sediments. *Geochimica et Cosmochimica Acta*, *75*(20), 5903–5926. https://doi.org/10.1016/j.gca.2011.07.046

Villa, I. M., De Bièvre, P., Holden, N. E., & Renne, P. R. (2015). IUPAC-IUGS recommendation on the half life of 87Rb. *Geochimica et Cosmochimica Acta*, *164*, 382–385. https://doi.org/10.1016/j.gca.2015.05.025

Weber, B., Schmitt, A. K., Cisneros de León, A., & González-Guzmán, R. (2019). Coeval early ediacaran breakup of Amazonia, Baltica, and Laurentia: Evidence from micro-baddeleyite dating of dykes from the Novillo canyon, Mexico. *Geophysical Research Letters*, *46*(4), 2003–2011. https://doi.org/10.1029/2018gl079976

Williams, C. D., Li, M., McNamara, A. K., Garnero, E. J., & van Soest, M. C. (2015). Episodic entrainment of deep primordial mantle material into ocean island basalts. *Nature Communications*, *6*(1), 8937. https://doi.org/10.1038/ncomms9937

Williams, M. J., Schoneveld, L., Mao, Y., Klump, J., Gosses, J., Dalton, H., et al. (2020). pyrolite: Python for geochemistry. *The Journal of Open Source Software*, *5*(50), 2314. https://doi.org/10.21105/joss.02314

Williamson, N. M. B., Weis, D., Scoates, J. S., Pelletier, H., & Garcia, M. O. (2019). Tracking the geochemical transition between the kea-dominated northwest Hawaiian ridge and the bilateral loa-kea trends of the Hawaiian islands. *Geochemistry, Geophysics, Geosystems*, *20*(9), 4354–4369. https://doi.org/10.1029/2019gc008451

Wolf, J., & Evans, D. A. D. (2021). Reconciling supercontinent cycle models with ancient subduction zones. *Earth and Planetary Science Letters*, *578*, 117293. https://doi.org/10.1016/j.epsl.2021.117293

Woodhead, J., Hergt, J., Giuliani, A., Maas, R., Phillips, D., Pearson, D. G., & Nowell, G. (2019). Kimberlites reveal 2.5-billion-year evolution of a deep, isolated mantle reservoir. *Nature*, *573*(7775), 578–581. https://doi.org/10.1038/s41586-019-1574-8

Woodhead, J., Hergt, J., Phillips, D., & Paton, C. (2009). African kimberlites revisited: In situ Sr-isotope analysis of groundmass perovskite. *Lithos*, *112*, 311–317. https://doi.org/10.1016/j.lithos.2009.03.031

Woodland, A. B., Kornprobst, J., McPherson, E., Bodinier, J. L., & Menzies, M. A. (1996). Metasomatic interactions in the lithospheric mantle: Petrologic evidence from the lherz massif, French pyrenees. *Chemical Geology*, *134*(1), 83–112. https://doi.org/10.1016/s0009-2541(96)00082-4

Xu, J.-Y., Giuliani, A., Li, Q. L., Lu, K., Melgarejo, J. C., & Griffin, W. L. (2021). Light oxygen isotopes in mantle-derived magmas reflect assimilation of sub-continental lithospheric mantle material. *Nature Communications*, *12*(1), 6295. https://doi.org/10.1038/s41467-021-26668-z

Yan, J., Ballmer, M. D., & Tackley, P. J. (2020). The evolution and distribution of recycled oceanic crust in the Earth's mantle: Insight from geodynamic models. *Earth and Planetary Science Letters*, *537*, 116171. https://doi.org/10.1016/j.epsl.2020.116171

Yang, Y.-H., Wu, F. Y., Wilde, S. A., Liu, X. M., Zhang, Y. B., Xie, L. W., & Yang, J. H. (2009). In situ perovskite Sr–Nd isotopic constraints on the petrogenesis of the Ordovician Mengyin kimberlites in the North China Craton. *Chemical Geology*, *264*(1–4), 24–42. https://doi.org/10.1016/j.chemgeo.2009.02.011

Yaxley, G. M., Berry, A. J., Rosenthal, A., Woodland, A. B., & Paterson, D. (2017). Redox preconditioning deep cratonic lithosphere for kimberlite Genesis – Evidence from the central Slave Craton. *Scientific Reports*, *7*(1), 30. https://doi.org/10.1038/s41598-017-00049-3

Young, A., Flament, N., Maloney, K., Williams, S., Matthews, K., Zahirovic, S., & Muller, R. D. (2019). Global kinematics of tectonic plates and subduction zones since the late Paleozoic Era. *Geoscience Frontiers*, *10*(3), 989–1013. https://doi.org/10.1016/j.gsf.2018.05.011

Zindler, A., & Hart, S. (1986). Chemical geodynamics. *Annual Review of Earth and Planetary Sciences*, *14*(1), 493–571. https://doi.org/10.1146/annurev.ea.14.050186.002425

References From the Supporting Information

Kavanagh, J. L., & Sparks, R. S. J. (2009). Temperature changes in ascending kimberlite magma. *Earth and Planetary Science Letters*, *286*(3), 404–413. https://doi.org/10.1016/j.epsl.2009.07.011